Groundwater Research Report
WR92R003

FIELD EVALUATION OF NEAR SOURCE TRANSPORT OF CONTAMINANTS IN HETEROGENEOUS MEDIA

John A. Hoopes
Salwa Rashad
Yahia Majali
Tswn-Syau Tsay

Funding Year: 1992

Final Project Report

for

"Field Evaluation of Near Source Transport of Contaminants in Heterogeneous Media"

to

Wisconsin Water Resources Center

from

John A. Hoopes, Professor
Salwa Rashad, Assistant Scientist
Yahia Majali, graduate student
Tswn-Syau Tsay, graduate student

Civil and Environmental Engineering Department
University of Wisconsin
1415 Johnson Drive
Madison, WI 53706

for

July 1, 1992- June30, 1994

Table of Contents

List of Figures and Tables

Tables

Figures

Abstract

This project extended the investigation "Near Source Transport of Contaminants in Hetergeneous Media" of contaminant plume and groundwater mounding behavior by applying this work to a field site. As geologic and aquifer properties are known only at a finite number of locations, kriging is used to estimate properties at all locations. Stochastic and deterministic models are used in conditional simulations to predict flow field and mounding behavior. The goals of this project were to :(1) use conditional Monte Carlo simulation to predict the regional flow field at one field site (Lake Geneva recharge facility) with existing data;(2) assess uncertainty in prediction of mound or plume behavior (using existing models) due to imperfect knowledge of hydrogeologic parameters;(3) evaluate the effects of additional field measurements of aquifer parameters (e.g., hydraulic conductivity) on the uncertainty of predictive variables (e.g., mounding height and plume penetration); and (4) establish a tool for use at other field sites and investigate the effects of design and operating alternatives and seasonal variability on mounding and plume behavior.

The methods and accomplishments from this work are presented in two parts. In part I, aquifer properties were estimated from kriging (first using hydraulic conductivity (K) data and second using soil type (ST) data with a triangular distribution for K and each ST). Then two groundwater flow models were run to simulate the water table with and without recharge and compared with observations. Results with the 2-dimensional, finite element AQUIFEM model showed that additional data on heterogeneity and K and a 3-dimensional model were needed. One simulation (realization) with the 3-dimensional MODFLOW model gave a similar pattern and comparable magnitudes to the observations. Multiple realizations are needed to assess uncertainty, and the plume model needs to be run to test it with the data. In part II, a numerical method to simulate two- and three-dimensional, transient groundwater mounding was developed and tested with a Hele-Shaw model. The boundary of the recharged water was determined by a particle tracking. The effects on mounding of the geometry, position, orientation and hydraulic conductivity of a single heterogeneity were computed. Three-dimensional results and application to the field site are in progress.

Introduction

Groundwater contaminant distributions from waste spills, landfill and storage facility leaks, and recharged surface water generally exhibit spatial and temporal variability due to geologic, regional flow and source property variations. To protect "clean" groundwater or to cleanup "contaminated" groundwater knowing the flow pattern is a key first step in determining the contaminant distribution and its movement.

In this project a method (kriging with hydraulic conductivity (K) and kriging with soil type (ST) and a triangular, probability distribution for K for each ST) for estimating aquifer properties at all locations from a limited numbers of observations is applied to the treated wastewater recharge facility at Lake Geneva, WI. Using estimated K values, the water table with and without recharge is simulated with two- and three-dimensional steady, numerical models and compared to observations. In addition, a general, three-dimensional, transient, numerical model, using grid transformation, for predicting mounding in heterogeneous aquifers is developed and tested. The methods results, and conclusions and recommendations from this work are presented in two parts.

I. Estimation of Flow Parameters and Simulation of Water Table Elevations

1.1 Kriging with Hydraulic Conductivity and Two-Dimensional Simulation

1.1.1 Introduction

Contaminant transport is strongly affected by stratigraphic and lithological variations of material properties (Anderson, 1987). Generally aquifer properties are known only at a finite number of locations; hence, an estimation algorithm is needed to define the hydraulic properties at all points. These properties are input parameters in regional flow models (Phillips, 1989). Numerical models of groundwater and solute transport are increasingly used to investigate critical environmental problems such as groundwater supply, groundwater contamination, and the design of subsurface disposal and remediation facilities. While these numerical models are generally sophisticated, their input flow parameters are often poorly known (Ahmed and Marsily, 1989). Awareness of this imbalance and the need to improve the predictive ability of numerical flow models have prompted significant research for characterizing heterogeneous geologic media. In this report, kriging is used to obtain estimates of hydraulic conductivity underneath the Lake Geneva wastewater, rapid infiltration site; these values are used in a 2-dimensional groundwater flow model to predict the water table elevations, which are compared to observed values.

1.1.2 Aquifer and Flow Field Properties

The 8 dosing cells at the rapid infiltration site in the City of Lake Geneva, Wisconsin are shown in Figure 1.1. The site is situated on an unconfined, glacial outwash aquifer, comprised of discontinuous strata of gravel, interbedded very sandy gravel, and gravel, sands, silts, and clays. The gravel deposits range in thickness from 15-35 feet in the northern half of the site to 5-20 feet in the southern half of the site. Groundwater flows from west to east across

the site where it discharges into a marshland and river. The average water table gradient is 0.005. No significant vertical gradient was noted in the monitoring wells. A geotechnical report, published by the City of Lake Geneva (1984), indicates a hydraulic conductivity range of 80 ft/day to 400 ft/day for this region of Walworth County. Pump tests were conducted at the site by the City of Lake Geneva, using the modified well equation; horizontal, hydraulic conductivities in the range of 14.7 to 106.0 ft/day were obtained. From grain size analyses on soil samples, hydraulic conductivity values for the subsurface materials were estimated. The D_{10} (10 percent fine) size and P_{200} (percent passing No. 200 sieve) of these samples were compared to various empirical hydraulic conductivity charts. To gain more confidence, we conducted slug tests on the available 23 monitoring wells at the site using pressure transducers and Hermit data loggers. The data and analysis of these tests are available in the project file. The weighted average value for the horizontal hydraulic conductivity, $\sum K_{h_i} L_i / \sum L_i$, where L_i = screen length, from the slug tests is 12.8 ft/day; K_h ranges from 0.7 to 773 ft/day Table 1.1. The slug tests results are treated as hard data in the kriging.

1.1.3 Approach

The observed water table data are plotted in Figure 1.1. These water table contours represent conditions before dozing of the seepage cells began. The model verification and calibration will be based on comparison with Figure 1.1.

Initially a 2-dimensional, vertically-integrated approach was used to simulate the water table and flow field. A 2-dimensional, finite element mesh was constructed and simulations were done using AQUIFEM (Townley and Wilson, 1980). The hydraulic conductivity at each node for every cell was estimated by constructing variograms along the major and minor axes of the hydraulic conductivity. The major axis was found in the N60°E direction while a minor axis was found in the N30°W. Spherical models for the variograms of LnK in the form (Journal and Huijbregets, 1978), were fitted in the form:

$$\gamma(r) = \begin{Bmatrix} \frac{3}{2}\frac{r}{a} - \frac{1}{2}\frac{r^3}{a^3}, \forall r \in [0,a] \\ 1 = \text{sill}, \forall r \geq a \end{Bmatrix}, \qquad (1.1)$$

where r = lag distance and a = range.

Figure 1.2 shows the measured and fitted variograms in the N60° E direction. The range for the fitted variogram is 1000 ft and the sill is 0.42 ft^2. On the other hand, the range for the N30° W is 600 ft and the sill is 0.6 ft^2, as shown in Figure 1.3. This analysis showed that the hydraulic conductivity has two types of anisotropy (geometric and zonal) in addition to heterogeneity.

The correlation functions in Figures 1.2 and 1.3 were used in the two-dimensional, anisotropic, ordinary kriging program to solve for estimated hydraulic conductivity values at each node of every finite element. The output from this estimation is plotted in Figure 1.4. The values of the estimated hydraulic conductivities were used as an input parameters in AQUIFEM. The results of the simulation are plotted in Figure 1.5.

1.1.4 Discussion and Conclusions

The simulation results in Figure 1.5 are in reasonable agreement with the large scale features of the water table elevations from field measurements in Figure 1.1. Hydraulic conductivity data collected from the field were insufficient to accurately define the correlation function. Lack of field measurements of water table elevation also contributed to differences between observed values and the numerical model results. Other parameters in the model (e.g., boundary conditions, elevation of the aquifer bottom) affected the results of the simulation. The available data from this site is typical of the amount of hard data commonly available. The next step in the study was to combine other sources of geologic data to develop a better understanding of the heterogeneity at this site. In this step a method to integrate measurements of hydraulic conductivity, soil characteristics, and geologic information was used in order to characterize the hydraulic conductivity distribution.

1.2 Kriging with Soil Type and Three-Dimensional Simulation

1.2.1 Characterization of Site

Available information about the site was collected with the assistance of Mr. Bill Phillips (Water Resources Bureau, Department of Natural Resources in Wisconsin-Madison). The collected data included: boring logs; fence diagrams; geological cross sections; maps (test borings, observation wells, monitoring wells, ground water contours);and available estimations of site hydraulic conductivity. Details of the site investigation are given in a Geotechnical Report prepared for the site by Donhue (1984). This information was evaluated and organized to give a representation of the geologic features, soil properties, and ground water conditions at Lake Geneva.

Then, each geologic unit was assigned a numerical soil classification, using the integers 1-6. The integer and soil types are: (1) clean gravel; (2) coarse to medium sand; (3) fine sand; (4) silty sand; (5) clayey silt; and (6) clay. Cartesian coordinates of each test boring sample were identified using the fence diagram, topographical maps, and the geologic cross sections. Each boring was represented by a distribution of one or more of these 6 soil types with uniform thickness.

A triangular distribution (Figure 1.6) was used as a probability density function to describe the hydraulic conductivity for a given soil type (ST). The distribution is defined using an upper bound (K_{max}), a lower bound (K_{min}), and the peak of the density function (K_p). To select K_{max}, K_{min}, and K_p for each ST, the chart developed by Cooper (1993) was used (Table 1.2). This relationship between ST and K_p is illustrated in Figure 1.7 .

The hydraulic conductivity measurements at the site, obtained from slug tests, were used in Figure 1.7 to estimate ST and were compared with the observed ST from the borings.

Figures 1.8 and 1.9 show the location of borings using transformed coordinates (XN,YN,ZN), which are related to topographical map coordinates (Xmap, Ymap, Zmap) by

$$XN = Xmap - 2427754$$

$$YN = Ymap - 218856$$

$$ZN = Zmap$$

where XN, YN, and ZN are in feet. Zmap is the elevation in feet above MSL.

1.2.2 Spatial correlation structure

Several exploratory analyses were conducted on the available data sets of K and ST, (e.g., plotting histograms and contours). In order to determine spatial continuity several attempts for ST and for LnK were made to construct different types of variograms (e.g., semivariograms, covariance, pairwise relative variograms, and indicator variograms (Issaks and Srivistava 1989)). The best description of spatial continuity was obtained using the semivariogram of ST from boring information and data obtained from the estimated ST at K measurement locations.

The spatial correlation structure inherent in ST was determined by computing three-dimensional, anisotropic experimental variograms. A model was then fit to the experimental variograms. Experimental variograms were constructed using GAM3 from the GSLIB geostatistical library (Deutsh and Journel 1992). The experimental variograms were computed from

$$\gamma^*_{ST}(\mathbf{h}) = \frac{1}{2\,N(\mathbf{h})} \sum_{i=1}^{N(\mathbf{h})} [\, ST(x_i + \mathbf{h}) - ST(x_i) \,]^2, \qquad (1.2)$$

where $\gamma^*_{ST}(\mathbf{h})$ is the estimated semivariogram for ST, **h** is the separation vector, and N(**h**) is the number of data pairs with a separation vector of approximately **h**. By trial the best spatial description was constructed using a tolerance of 15° in the half window angle in X-Y plane and in the dip direction and allowing a maximum deviation in the separation distance equal to 25% in the horizontal direction and 50% in the vertical direction.

The principal axes for ST were identified by constructing a series of experimental variograms, each having a separation vector with a different orientation relative to the Cartesian coordinates XN, YN, ZN. The analysis gave horizontal principal axes oriented N30°W and N60°E. For the vertical direction, the principal axis coincided with the vertical (Z) axis, see Figures. 1.10.a, 1.10.b, and 1.10.c.

A spherical model with no nugget was found to give the best representation of the experimental semivariograms(Issaks and Srivistava 1989). The directional experimental semivariograms exhibit geometric anisotropy, which is characterized by different ranges and approximately the same sill C. To express the geometric anisotropy a standardized anisotropic variogram was used in the form

$$\gamma(h_1) = C[1.5(h_1) - 0.5(h_1)^3] \qquad \text{if } h_1 < 1 \qquad (1.3.a)$$

$$\gamma(h_1) = C \qquad \text{if } h_1 \geq 1 \qquad (1.3.b)$$

where $h_1 = \sqrt{\left(\frac{hx}{a_X}\right)^2 + \left(\frac{hy}{a_Y}\right)^2 + \left(\frac{hz}{a_Z}\right)^2}$, hx, hy and hz are the separation distances in X, Y, Z-directions, and a_X, a_Y, and a_Z are the ranges in the principal axes X, Y, Z, The best fit was obtained using C=2.8, a_X= 1600 ft, a_Y= 1232 ft, and a_Z=52 ft..

Kriging (Journel and Huijebregdts,1978, and Isaaks and Srivistava,1989) was used to estimate the ST field with the above correlation structure and the available ST data obtained directly from the boring tests or indirectly from the relationship between K and ST (Fig. 1.4) for each K measurement. At location X_o, $ST(X_o)$ is estimated from

$$ST(X_o) = \sum_{i=1}^{n} \alpha_i \, ST_i \quad , \tag{1.4}$$

where ST_i is the soil type value at location X_i , α_i is the averaging weight associated with the i^{th} data value. The weights are selected to ensure zero estimation bias and to minimize the variance of the estimation error, ε , given by

$$\varepsilon = ST(X_o) - ST_t(X_o) \tag{1.5}$$

where $ST_t(X_o)$ is the true value of soil classification at X_o, which is unknown. The geostatistical library "GSLIB" was used to construct a program for ordinary kriging (Deutsch and Journel (1992)) to obtain $ST(x_o)$ and e for every node of a regular three-dimensional grid.

The aquifer under the site is discretized into 2040 cells that comprise a finite-difference grid with 18 layers. Each layer contains 13 rows and 11 columns. Each cell is 200 feet in length and width and 8 feet in depth.

A cross validation technique was used to compare estimated and true values of ST. In cross validation, $ST_t(X_i)$ at a particular location X_i is temporarily discarded from the data set; the value at the same location is then estimated by $ST(X_i)$ using the remaining

data. When the estimate is calculated, it is compared to the true value that was initially removed from the data set. The residual at location X_i is

$$\text{Res}\ (X_i) = ST(X_i) - ST_t\ (X_i). \qquad (1.6)$$

This procedure was repeated for all available data. The resulting true and estimated values were then compared using statistical and visual tools.

Sensitivity analyses were conducted to test the influence of the fitted variogram model parameters (range and sill) and the estimation performance of the search strategy, defined by the search radius R and the maximum number of data points used in the estimation Nd. The sill was varied between 2 and 3, and the range in the principal direction was varied between 800 ft and 1600 ft. R was varied between 1000 ft and 1800 ft, and Nd was changed between 8 and 40. For each case, cross validation was implemented and the average and variance of the residual field were calculated. A spherical model with a_Y = 1600 ft, a_X= 1232 ft , a_z=53 ft , sill= 2.8, and R= 1800 ft with Nd= 8 gave the optimum results with enough data points to obtain the estimated ST field with residuals of minimum mean and variance. Figure 1.11 presents the residuals versus ST estimates and its statistics for the optimum case. The estimated ST field, using kriging, is shown in Figures 1.12.a, 1.12. b, 1.12.c.

1.2.3 Flow simulation

The three-dimensional finite difference program MODFLOW was used to simulate steady-state saturated flow in the aquifer below the site. The finite difference grid used to estimate the ST field was used in flow simulation. MODFLOW uses a block-centered finite difference scheme to solve the ground water flow equation. A detailed description of

MODFLOW can be found in MacDonald and Harbaugh (1988). MODFLOW was modified for use in this study by adding subprograms and changing the existing data collection and storage procedures. A subroutine "BOUNDARY" was developed to set up the boundary conditions and a subroutine "INHEAD" was developed to specify the initial value of the hydraulic head. A subroutine "HYCONAQ" was added to assign a hydraulic conductivity to each cell of the finite difference grid by employing the following procedure:

(1) Identify ST for a given cell using the output file of kriging simulation. Round this estimate to the nearest integer to select the corresponding parameters for the probability density function describing hydraulic conductivity (Table 1.2).

(2) Pick a random number F between 0 and 1 using a random number generator. In this study, the generator RAN1 was used (Press et al. 1986).

(3) Determine the hydraulic conductivity by inverting the random number F using:

$$\log K = \log K_{min} + \sqrt{F \log(K_{max} / K_{min}) \log(K_P / K_{min})}$$

$$\text{for } F \leq \frac{\log (K_p / K_{min})}{\log (K_{max} / K_{min})} \qquad (1.7)$$

or $$\log K = \log K_{max} - \sqrt{(1-F) \log(K_{max} / K_{min}) \log(K_{max} / K_P)}$$

$$\text{for } F > \frac{\log (K_p / K_{min})}{\log (K_{max} / K_{min})} \qquad (1.8)$$

This procedure was used to generate a single realization of the hydraulic conductivity field. Ground water flow was induced by applying an average hydraulic

gradient of 0.005 ft/ft, as reported in the Geotechnical report (1984) and as estimated from observation well data. Constant head boundary conditions were applied at the upstream and downstream planes (y-z). From the water table measurements, the constant heads were 856 ft upstream and 844 ft downstream. No flow boundaries were applied along the remaining surfaces of the aquifer. The aquifer layers were allowed to be saturated or unsaturated. A steady-state flow simulation was performed for two cases: (1) without recharge; and (2) with a uniform recharge rate of 0.00002 ft/s (equivalent to applying 1.7 MGD on seepage cell 5 which has an area of 120,000 ft^2, reported in Geotechnical report (1984)). Ground water elevations in the observation wells reported in table 1 of Geotechnical report (1984), were compared with computed ground water elevations at the observation wells to test the numerical model. Figure 1.13 illustrates the location of observation wells and cell 5. The measured water heads agreed well with the calculated ones using the steady-state flow simulation with no recharge, as shown in Figure 1.14. Figure 1.15 shows the comparison between water elevations computed for the steady flow with the uniform recharge rate and the measured ones. The discrepancy between the measured and calculated ones may be due to: (1) the measured heads may be taken in a different situation; (2) the recharge rate is not uniform over time as assumed in the computer simulation; (3) errors in representing the soil stratigraphy and properties; and (4) recharge and water table approximations in MODFLOW.

Elevations of ground surface at the observation wells are compared with the computed water elevations for the case where a uniform recharge is applied on cell 5, see Figure 1.16. The numerical results show that water elevations in wells 16, 17, and 20 are the closest to ground surface., which may imply that these wells need to be observed more often.

Contours of water table elevations obtained from the numerical simulations are shown in Figure 1.17 for the case without recharge, and in Fig. 1.18 for the case with recharge. Figure 1.18 illustrates the mounding effects near cell 5.

1.2.4 Conclusions and Recommendations

This study demonstrated that boring data for soil type can be used with a limited number of hydraulic conductivity measurements to estimate the hydraulic conductivity field, a key parameter for all ground water flow and contaminant transport models.

In this study only one realization of hydraulic conductivity field was used in the flow simulations. Results are in reasonable agreement with observations. Multiple realizations need to be done to quantify the uncertainty in the flow parameters. MODFLOW could be used to implement a simulation with loading of different seepage cells at different times to more accurately model this waste water recharge site.

Finally, using the hydraulic conductivity field generated in this work, the plume model (developed in an earlier phase of this work) and the mounding model (see Part II) could be used to estimate the movement, mixing and mounding of the recharged waste water.

References

Anderson, M. P., (1987), "Treatment of Heterogeneities in Ground water Flow Modeling in Solving Ground Water Problems with Models", (e. d. B. J. Graves) National Water Well Association, Dublin, Ohio, pp. 444-463.

Benson, C. and S. Rashad (1994), "Using Co-Kriging to Enhance Hydrogeologic Characterization," Environmental Geotechnics Report No. 94-1, Dept. of Civil and Environmental Engineering, University of Wisconsin, Madison, WI.

Cooper, S. and C. Benson (1993), "An Evaluation of How Subsurface Characterization Using Soil Classifications Affects Predictions of Contaminant Transport," Environmental Geotechnics Report No. 93-1, Dept. of Civil and Environmental Engineering, University of Wisconsin, Madison, WI.

Deutsch, C. and A. Journel (1992), *GSLIB Geostatistical Software Library and User's Guide Book,* Oxford University Press, New York.

Fogg, G. (1986), "Groundwater Flow and Sand Body Interconnectedness in a Thick, Multiple-Aquifer system," *Water Resources Research*, Vol. 22, No. 5, pp. 679-694.

Johnson, N. and S. Driess (1989), "Hydrostratigraphic Interpretation Using Indicator Geostatistics," *Water Resources Research,* Vol. 25, No. 12, pp. 2501-2510.

Journel, A. and C. Huijbregts (1978), *Mining Geostatistics*, Academic Press, London.

McDonald, M. and A. Harbaugh (1988), "A Modular Three-Dimensional Finite Difference Ground-Water Flow Model," *Techniques of Water-Resources Investigations of the United States Geological Survey,* USGS, Reston, VA.

Philips, F. M., (1984) , "An Approach to Estimating Hydraulic Conductivity Spatial Correlation Scales Using Geological Characteristics", WRR., vol. 25, no. 1, pp. 141-143.

"Rapid Infiltration System Geotechnical Report," City Of Lake Geneva, Wisconsin, August 1984.

Townley, L. R., and J. L. Wilson, (1980) "Description of and user's manual for a finite element aquifer flow model AQUIFEM, MIT Ralph M. Parsons Laboratory for Water Resources and Hydrodynamics, Technology Adaption Program Report No. 79-3.

Tables and Figures

Well No.	X-Axis (East)	Y-Axis (North)	Kh (ft/min)	Screen Length
1	2428895	220425	0.002095	5
2	2428895	220420	0.009408	9
3	2429137	219872	0.001885	9
4	2429500	219370	0.009911	10
5	2429450	220570	0.009726	9
6	2429860	220420	0.0040055	9
7	2429860	219970	0.004533	9
8	2429860	219965	0.003481	5
9	2429860	219570	0.001078	9
10	2430015	220786	0.001960	9
11	2430380	220700	*	9
12	2430380	220700	0.003313	5
13	2430400	220095	0.010930	10
14	2430450	219585	0.017960	5
15	2430450	219580	0.009396	9
16	*	*	*	*
17	2430999	220424	0.004935	10
18	2430871	219780	0.002380	5
19	2430871	219775	0.053710	9
20	2431100	219815	0.005993	5
21	2427854	220134	*	*
22	2430030	218956	*	*
23	2430030	218956	0.0005079	9

* - no test data

Table 1.1: Summary of slug tests results.

Soil Type	K_{min} (cm/sec)	K_p (cm/sec)	K_{max} (cm/sec)
Clean Gravel	5×10^{-1}	5×10^{0}	5×10^{2}
Coarse - Med.Sand	1×10^{-3}	5×10^{-2}	1×10^{0}
Fine Sand	1×10^{-4}	5×10^{-3}	5×10^{-2}
Silty Sand	5×10^{-5}	5×10^{-4}	5×10^{-3}
Clayey Silt	1×10^{-7}	1×10^{-6}	5×10^{-5}
Clay	1×10^{-10}	1×10^{-8}	1×10^{-6}

Table 1.2 Soil type and hydraulic conductivity parameters.

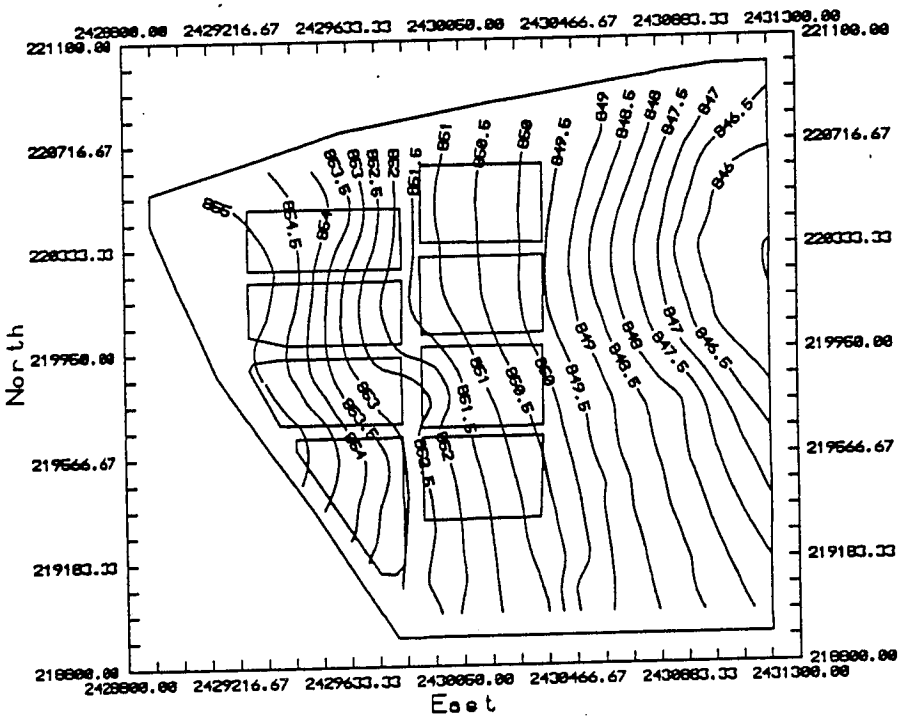

Figure 1.1: Measured water table elevation.

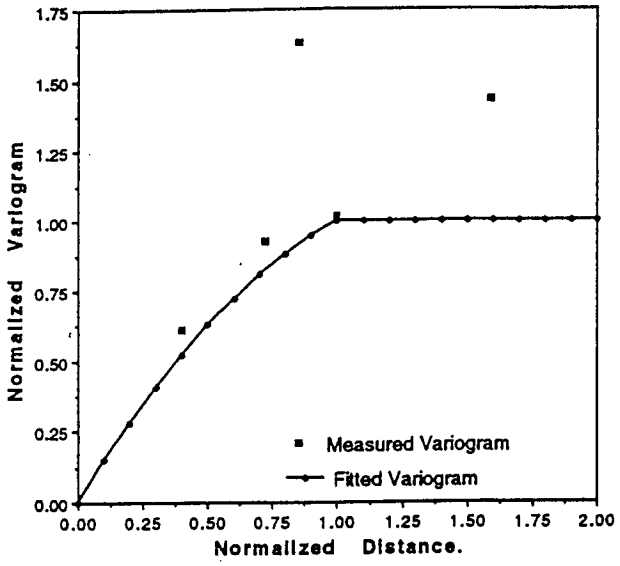

Figure 1.2: Measured and fitted variograms in the N60° E direction.

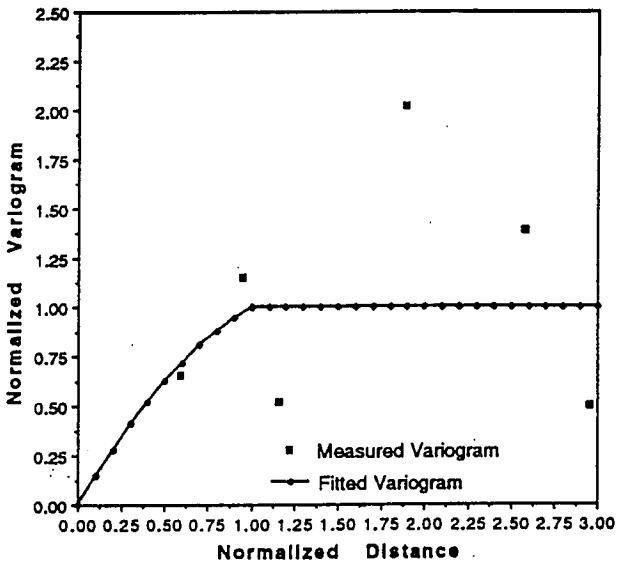

Figure 1.3: Measured and fitted variograms in the N30° W direction.

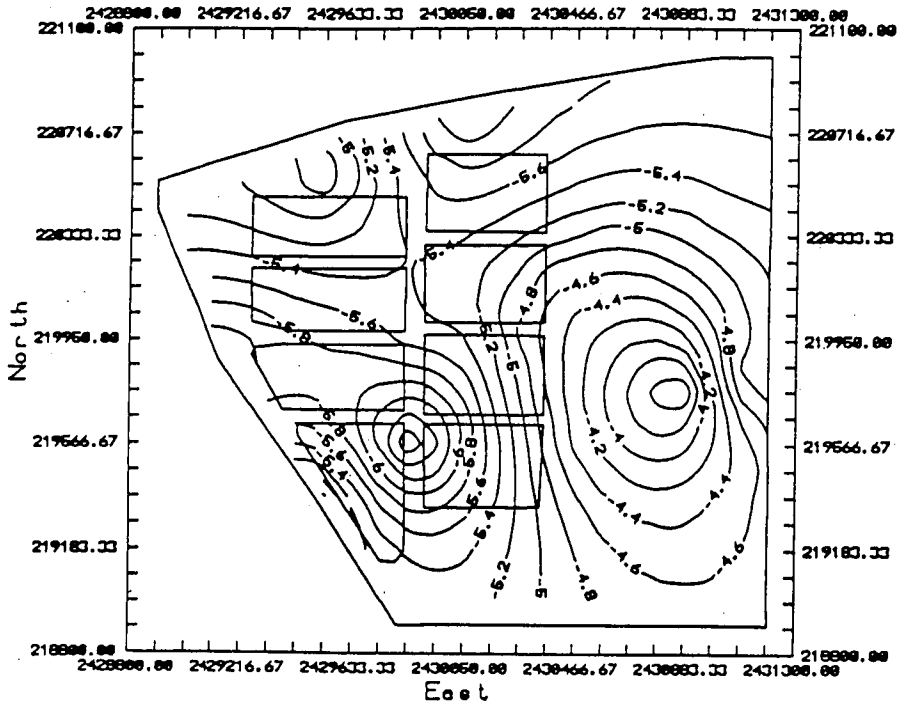

Figure 1.4: Contour map of the estimated Ln (K) ft/min.

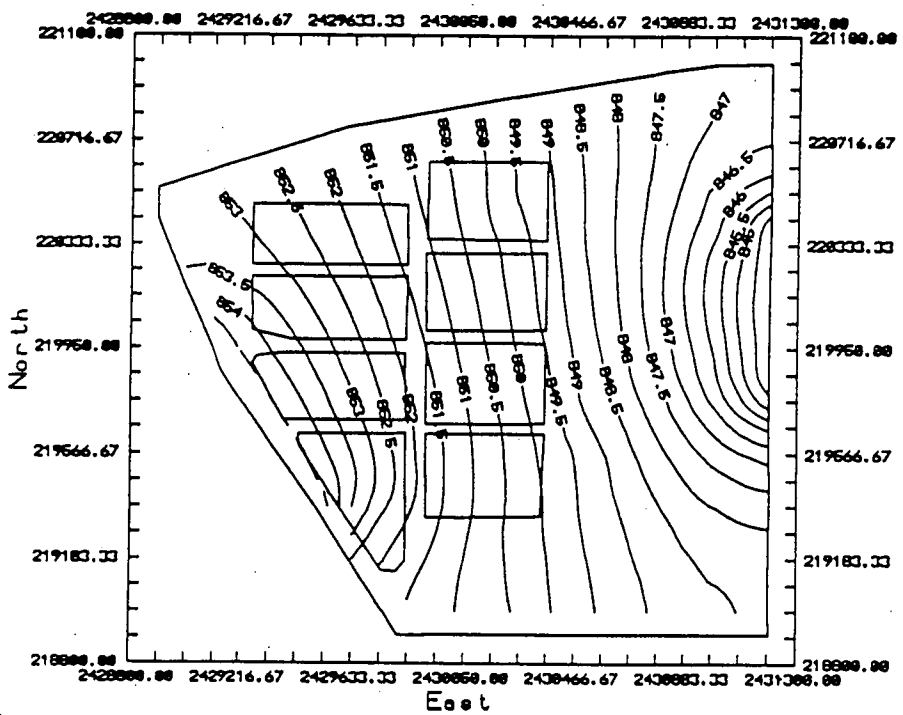

Figure 1.5: Simulated water table with the Kriged values for K.

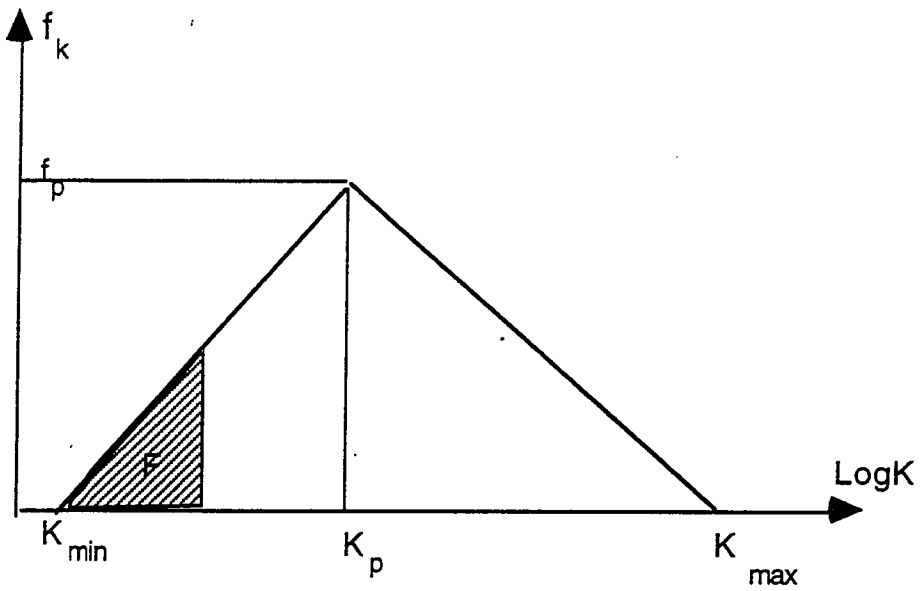

Fig. 1.6 Probability density function for hydraulic conductivity in a geologic unit.

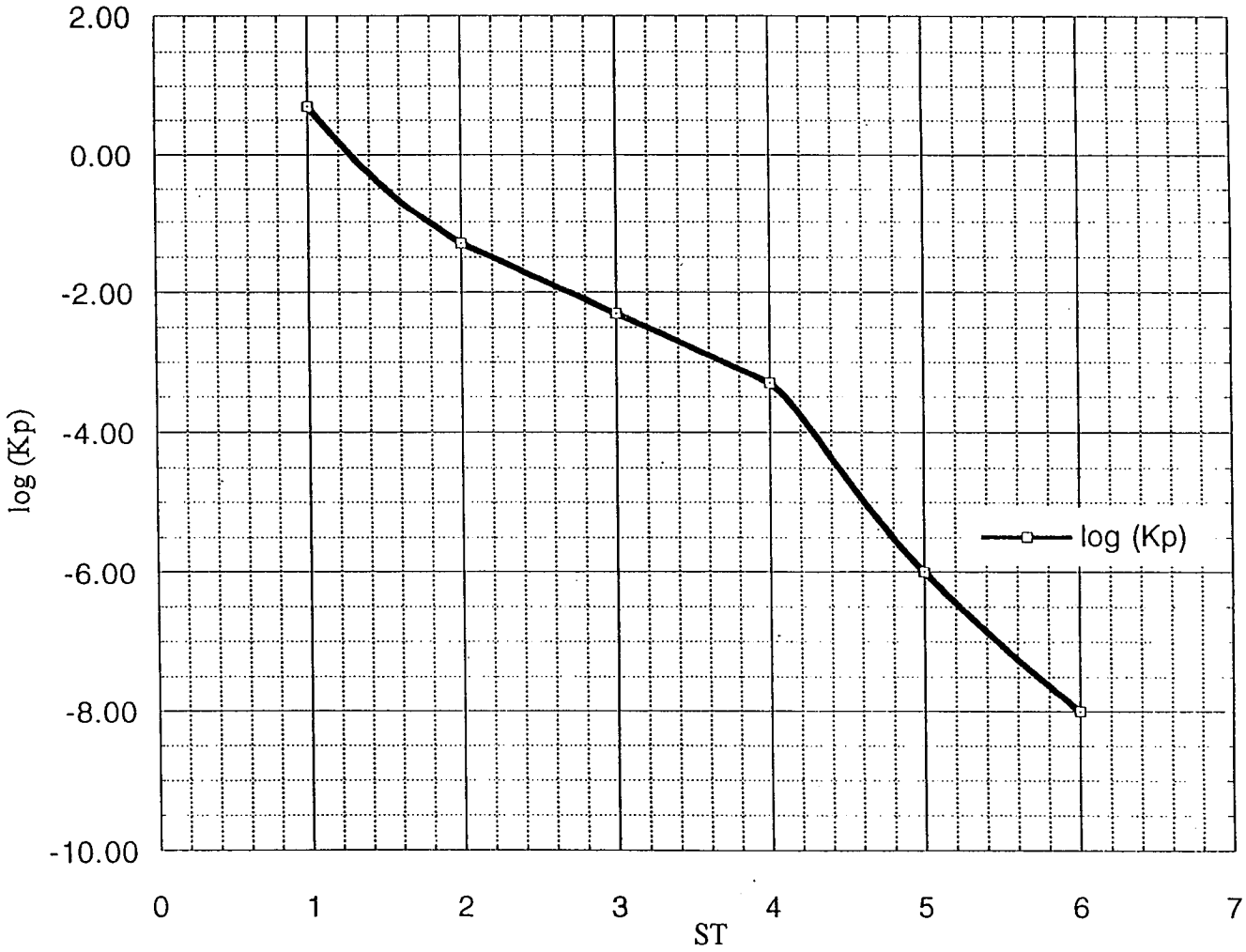

Fig. 1.7 Relationship between ST and log K_p

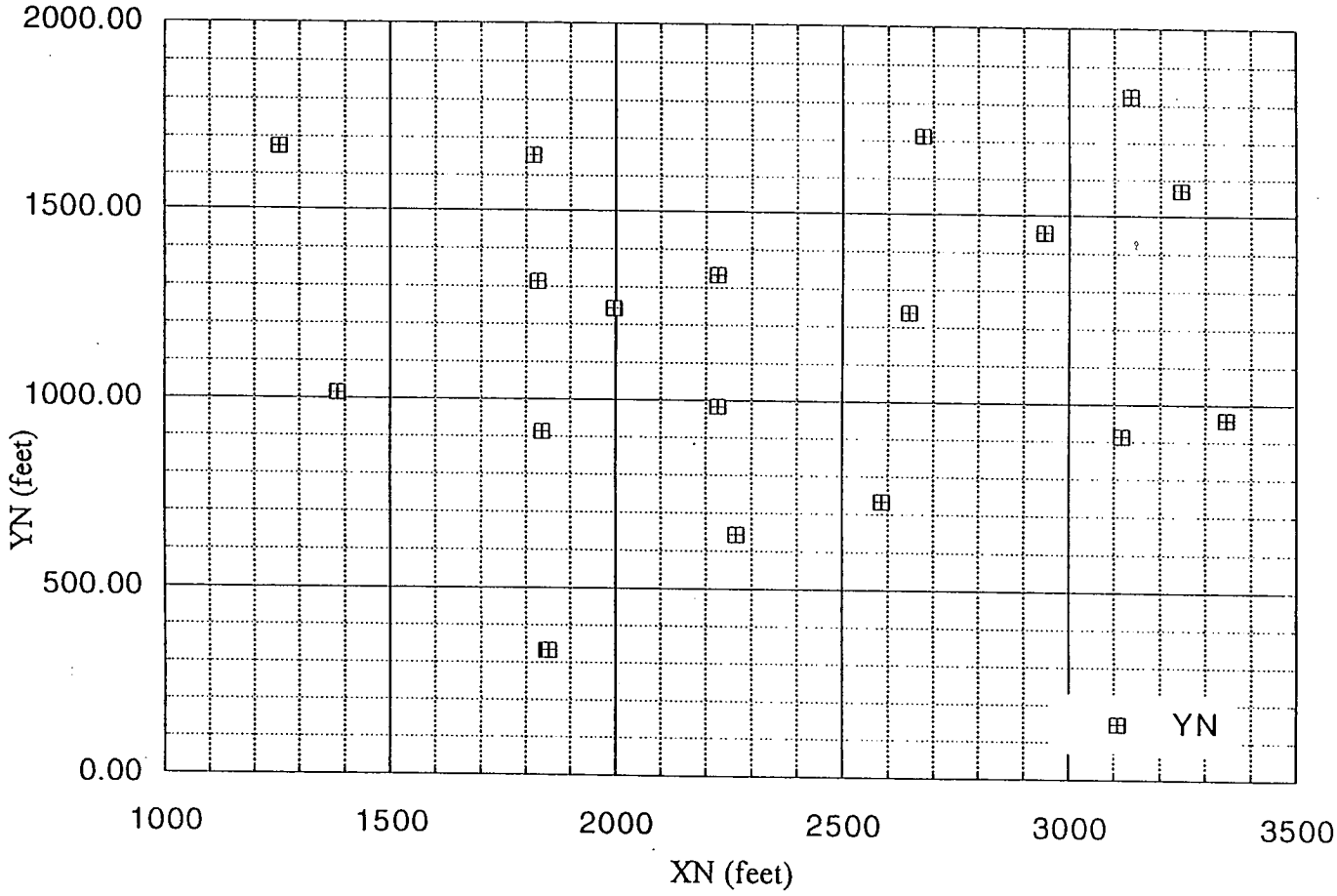

Fig. 1.8 Test boring locations in the horizontal plane XN, YN

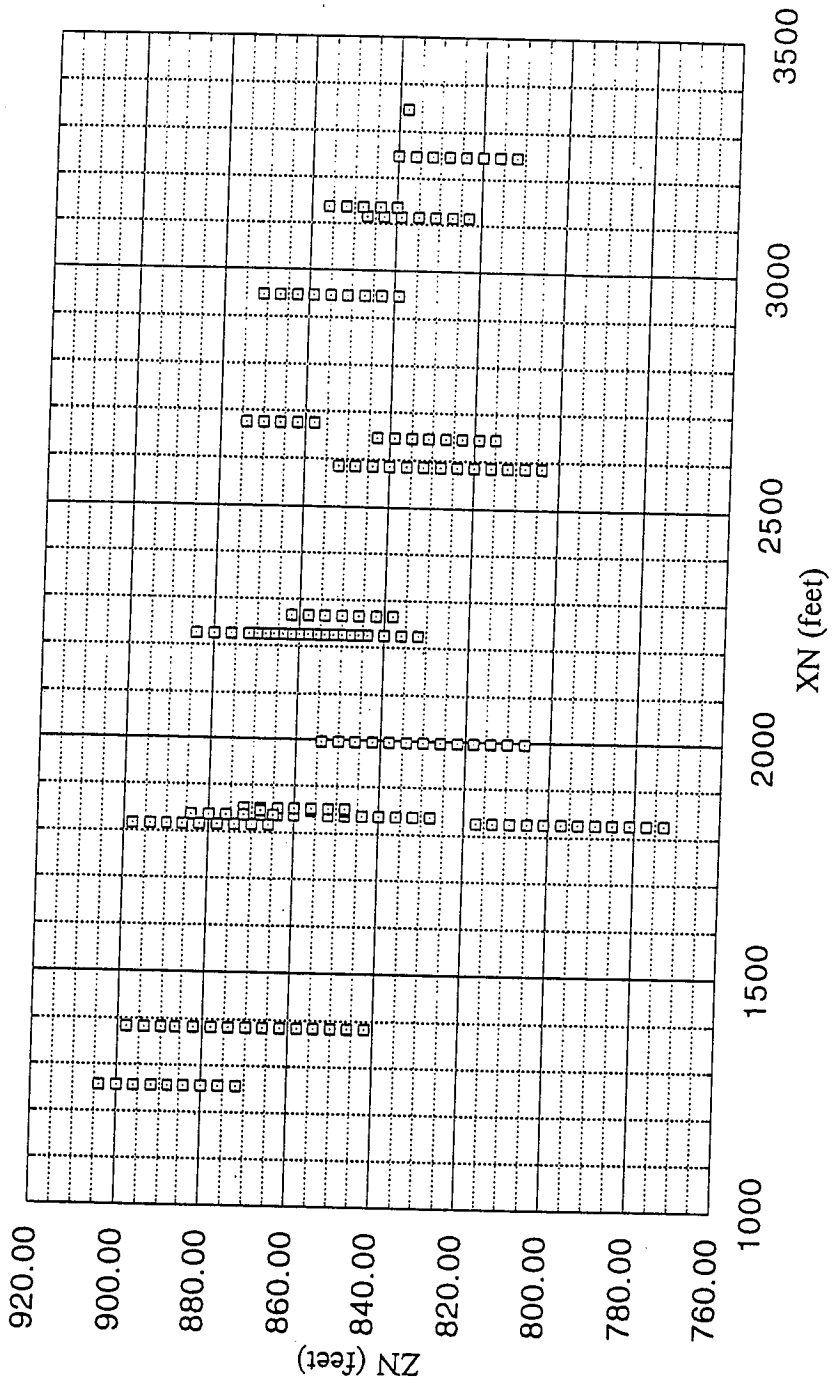

Fig. 1.9 Test boring locations in XN-ZN plane

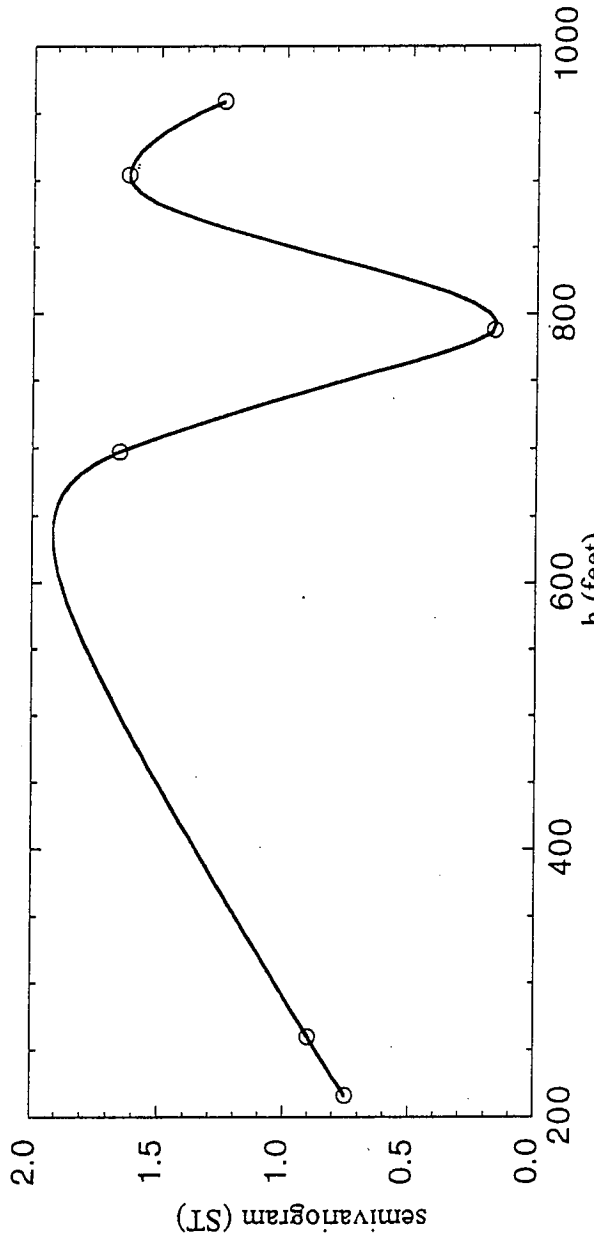

Fig. 1.10.a Experimental semivariograms in X direction (Xp = N30°W)

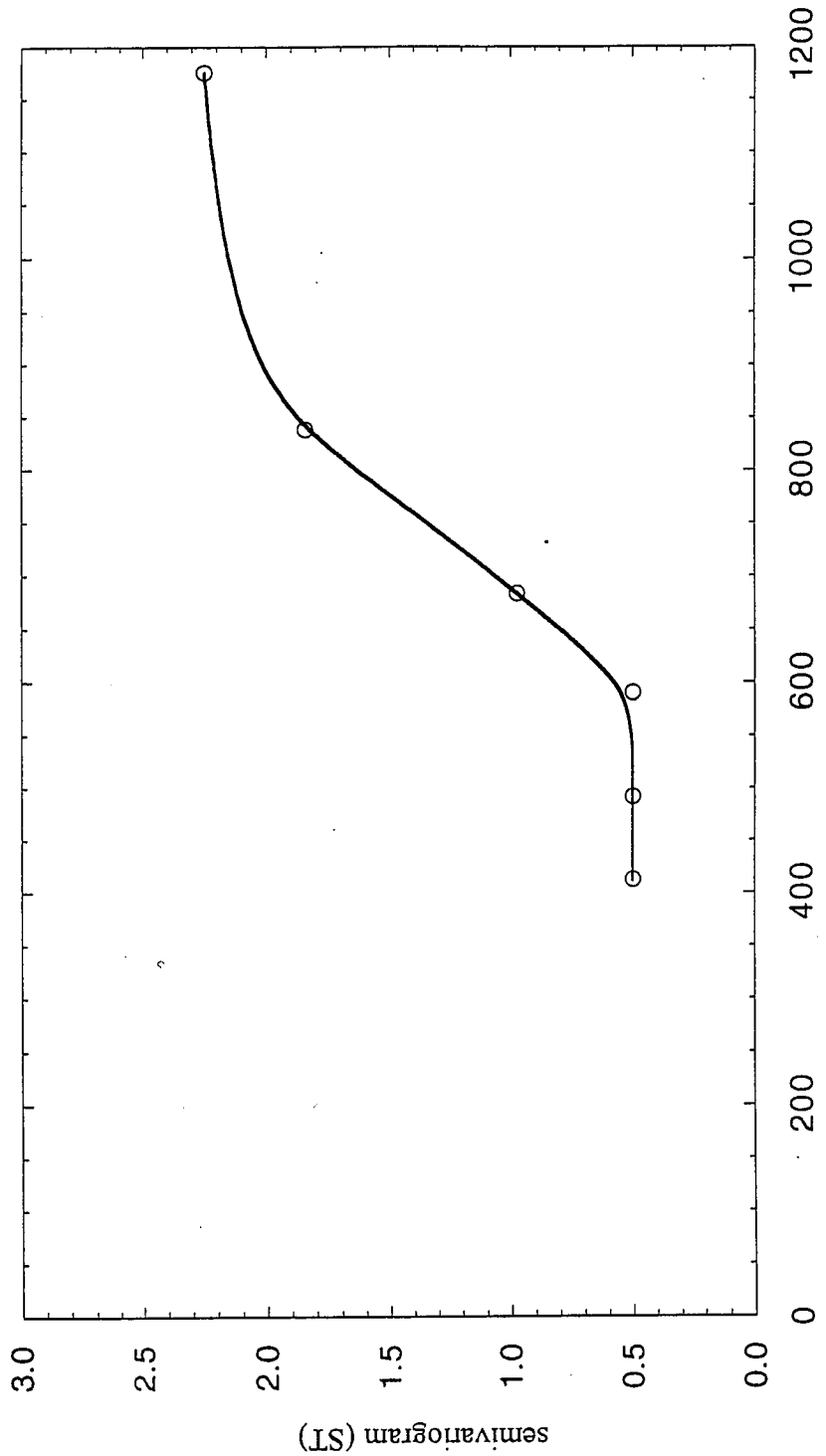

Fig. 1.10. b Experimental semivariograms in Y direction (Yp=N60°E)

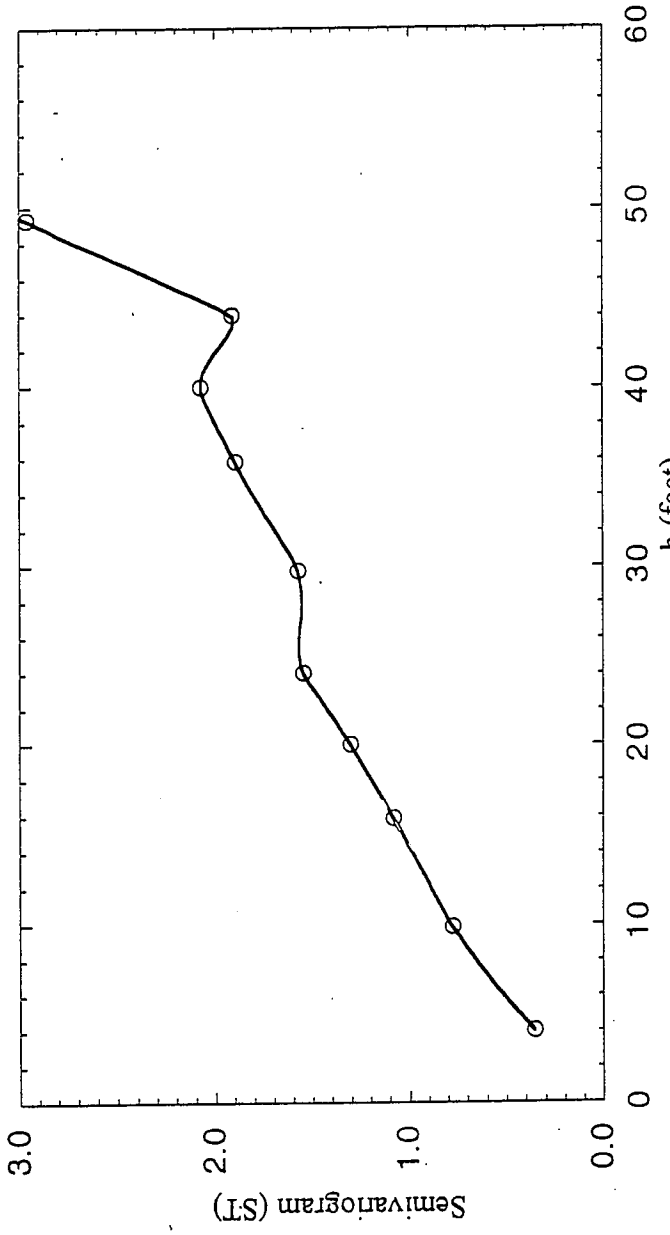

Fig. 1.10. c Experimental semivariogram in Z direction (Zp = vertical)

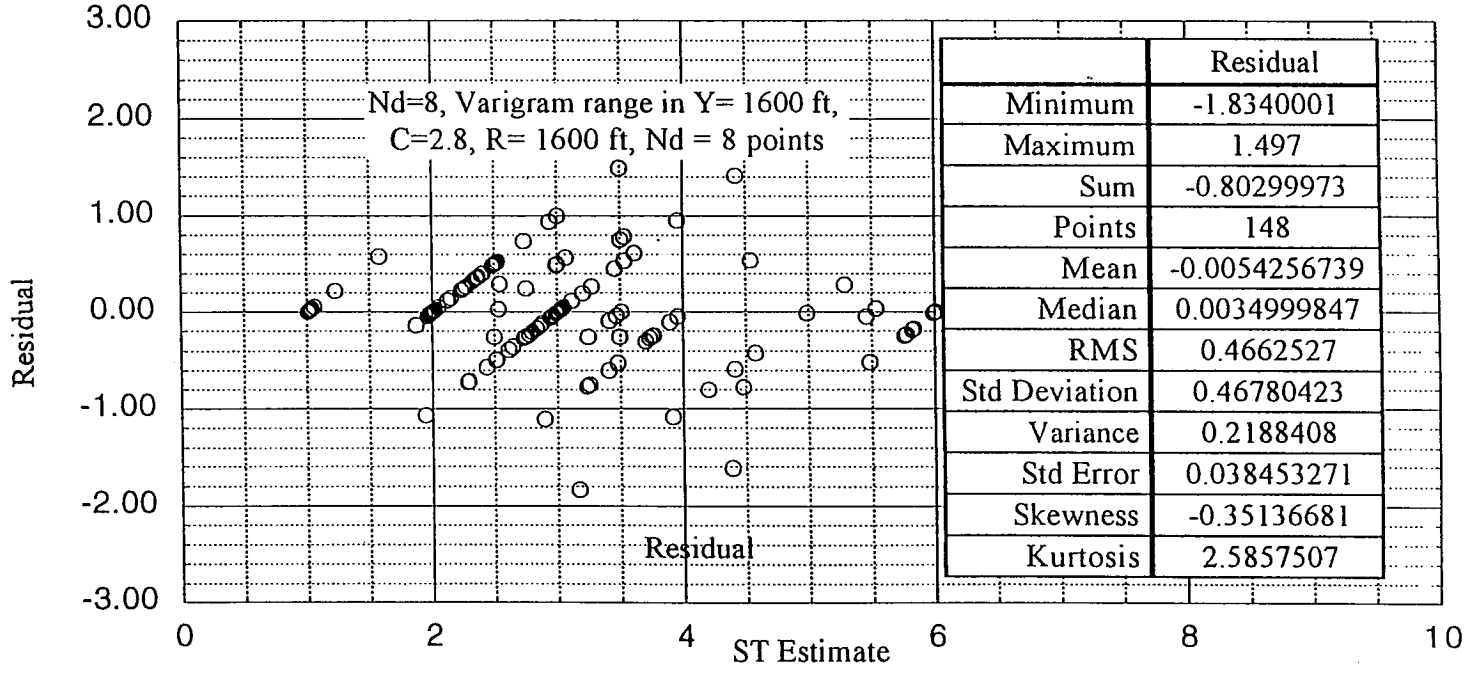

	Residual
Minimum	-1.8340001
Maximum	1.497
Sum	-0.80299973
Points	148
Mean	-0.0054256739
Median	0.0034999847
RMS	0.4662527
Std Deviation	0.46780423
Variance	0.2188408
Std Error	0.038453271
Skewness	-0.35136681
Kurtosis	2.5857507

Fig. 1.11 Residual field using cross validation

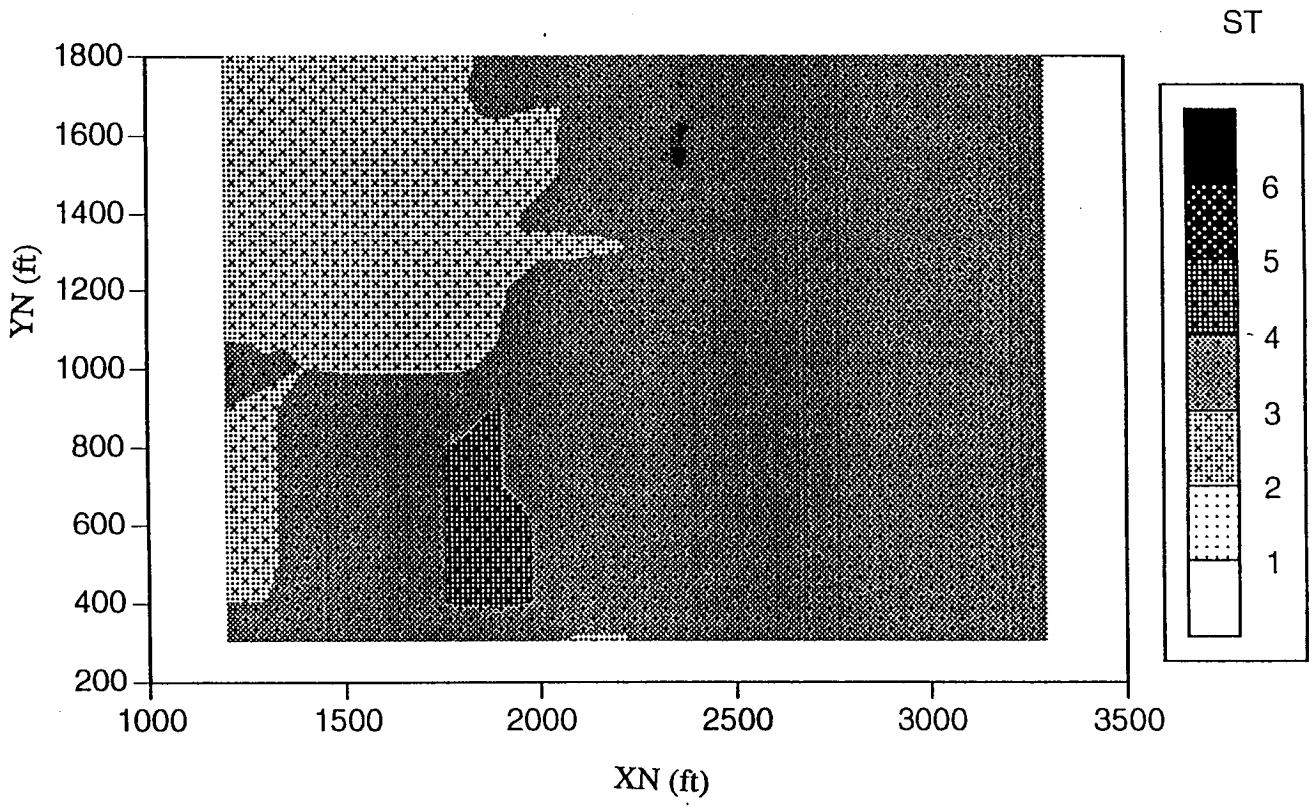

Fig.1.12.a Estimated ST field at ZN = 772 ft

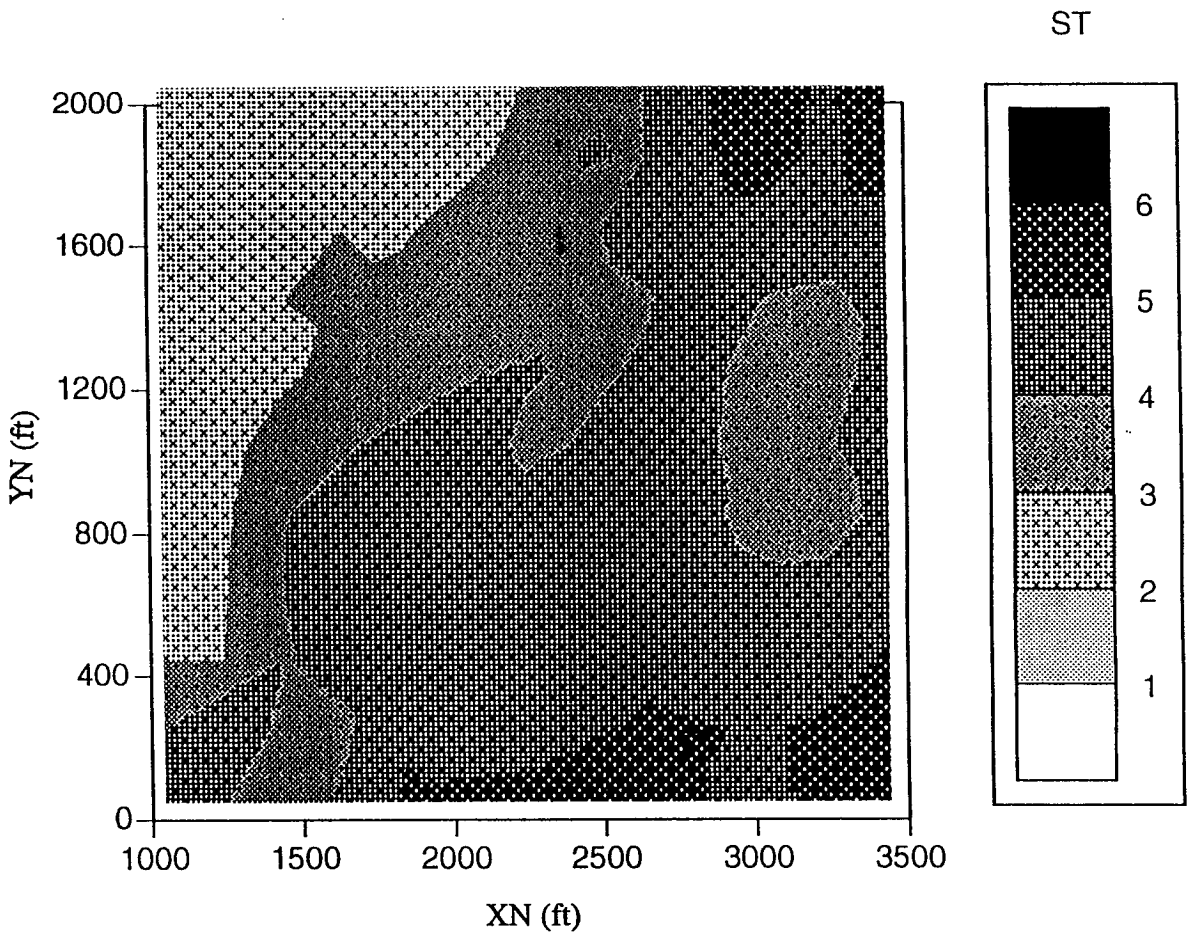

Fig. 1.12.b Estimated ST field at ZN = 812 ft

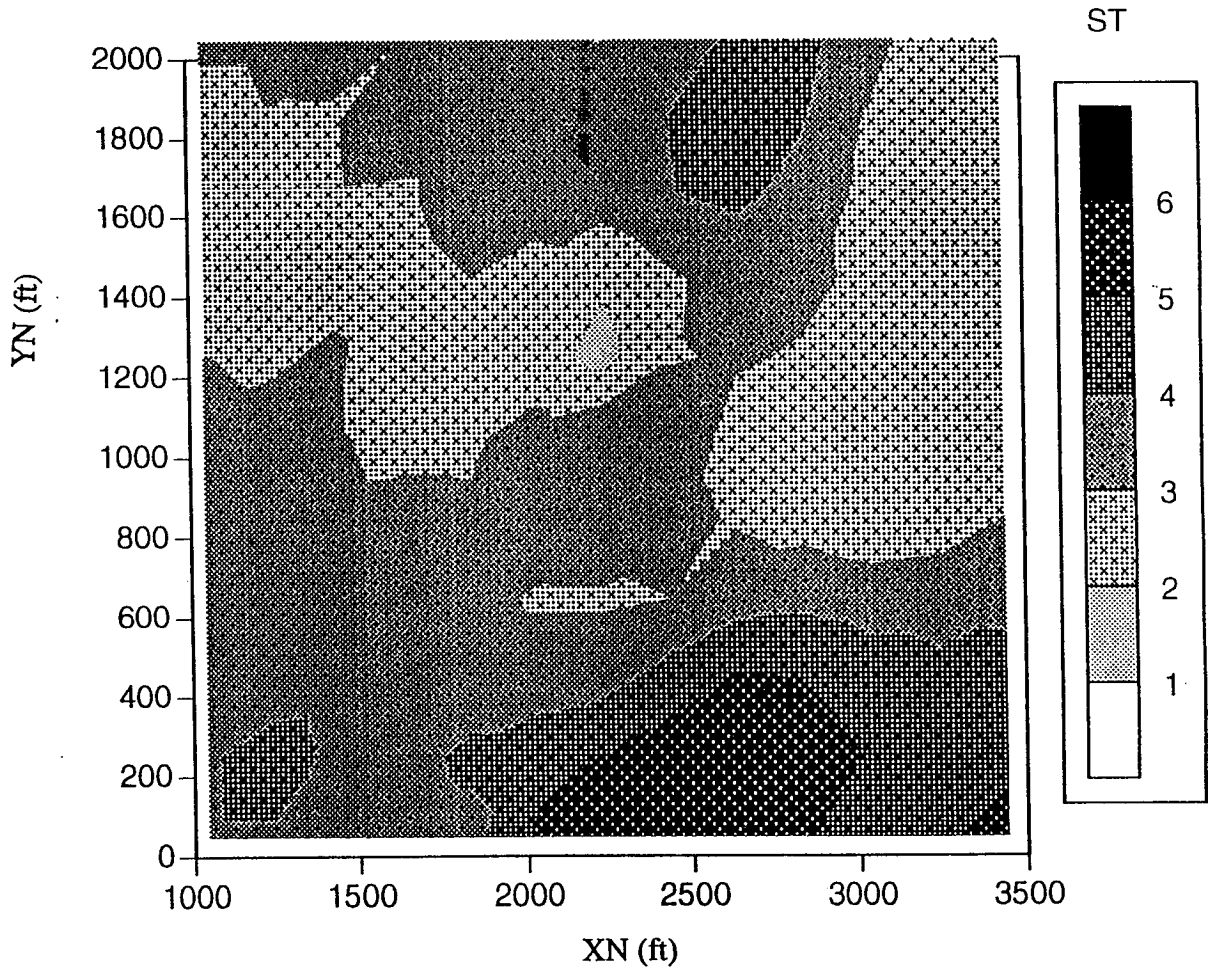

Fig. 1.12.c Estimated ST field at ZN = 852 ft

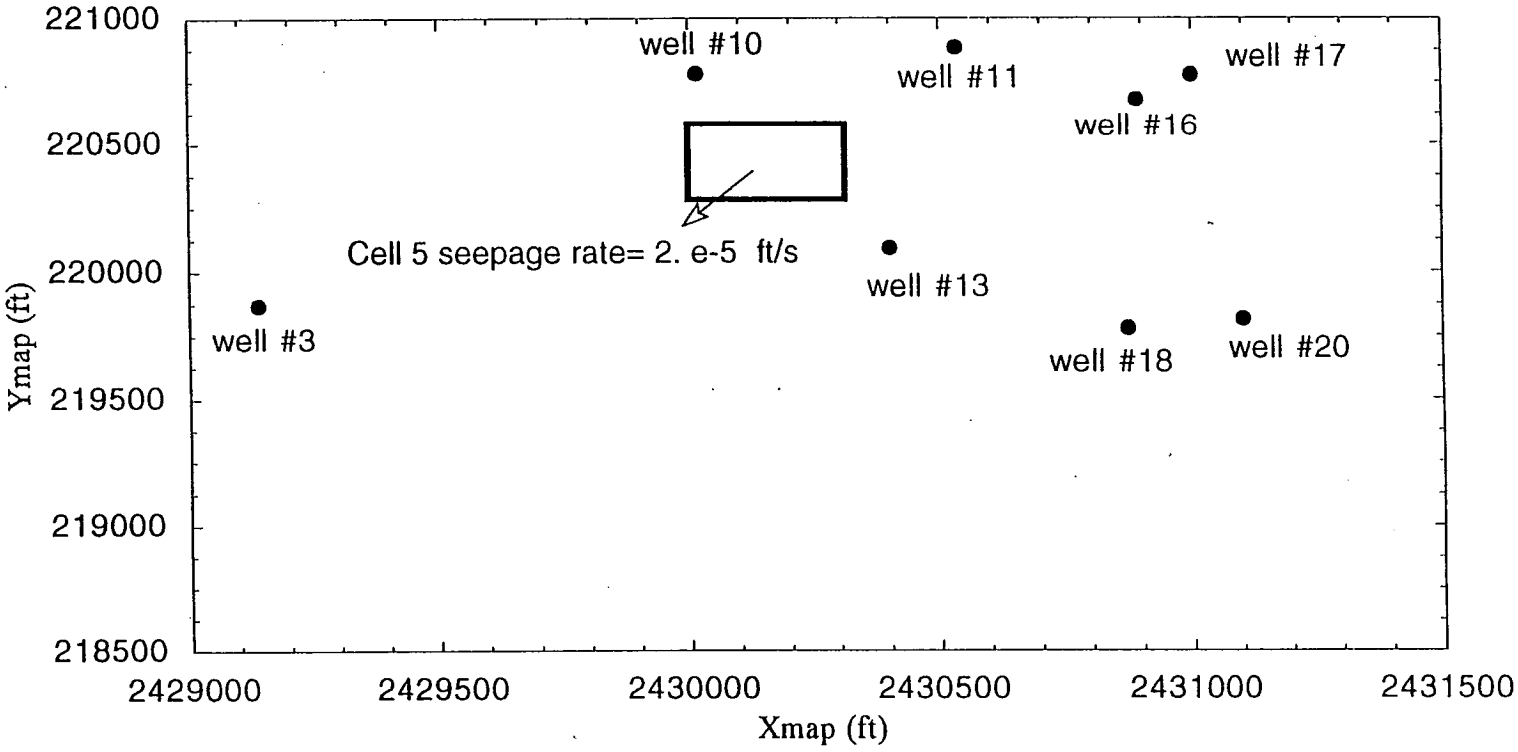

Fig. 1.13 Location of seepage cell 5 and observation wells

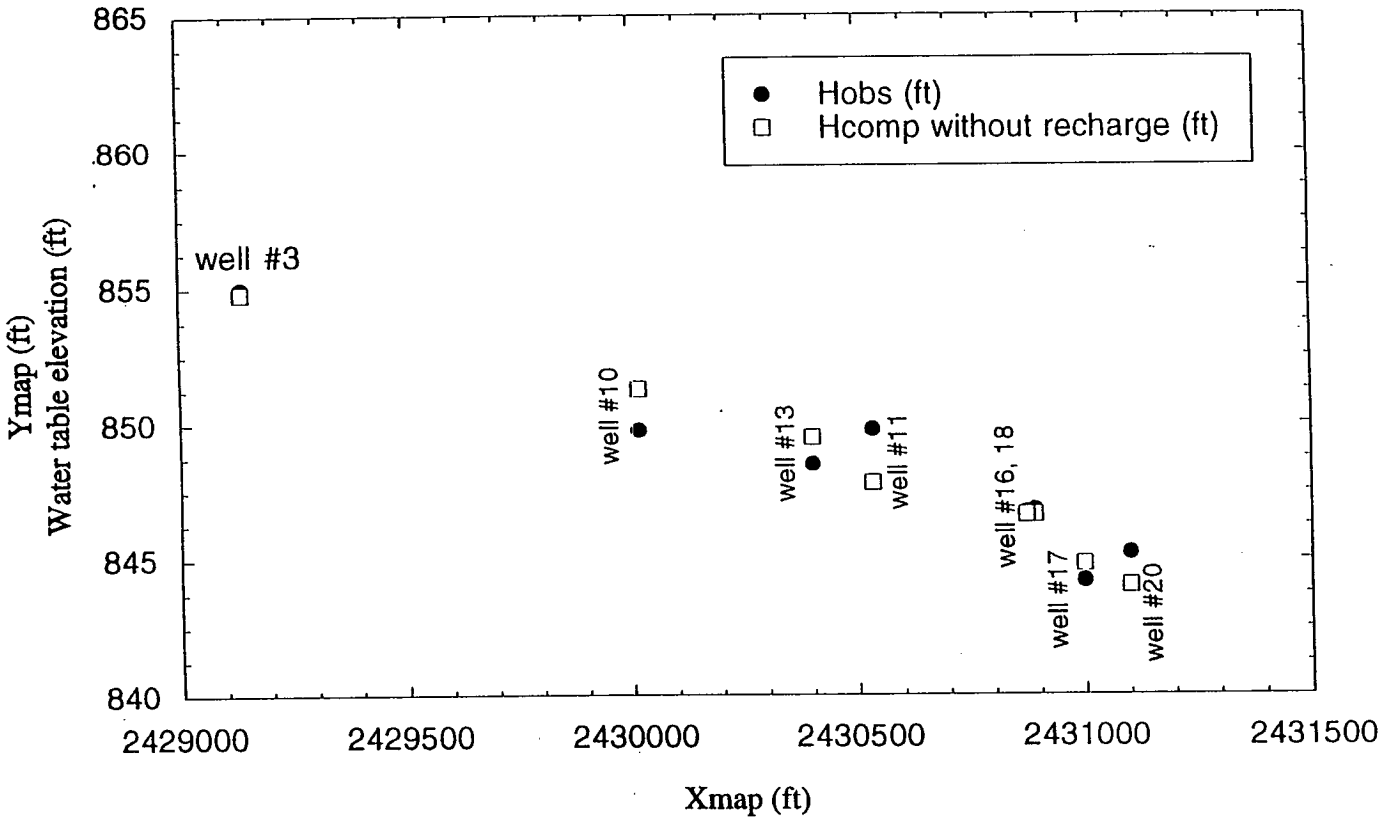

Fig. 1.14 Observed water elevation (Hobs) compared to computed water elevation (Hcomp) without recharge

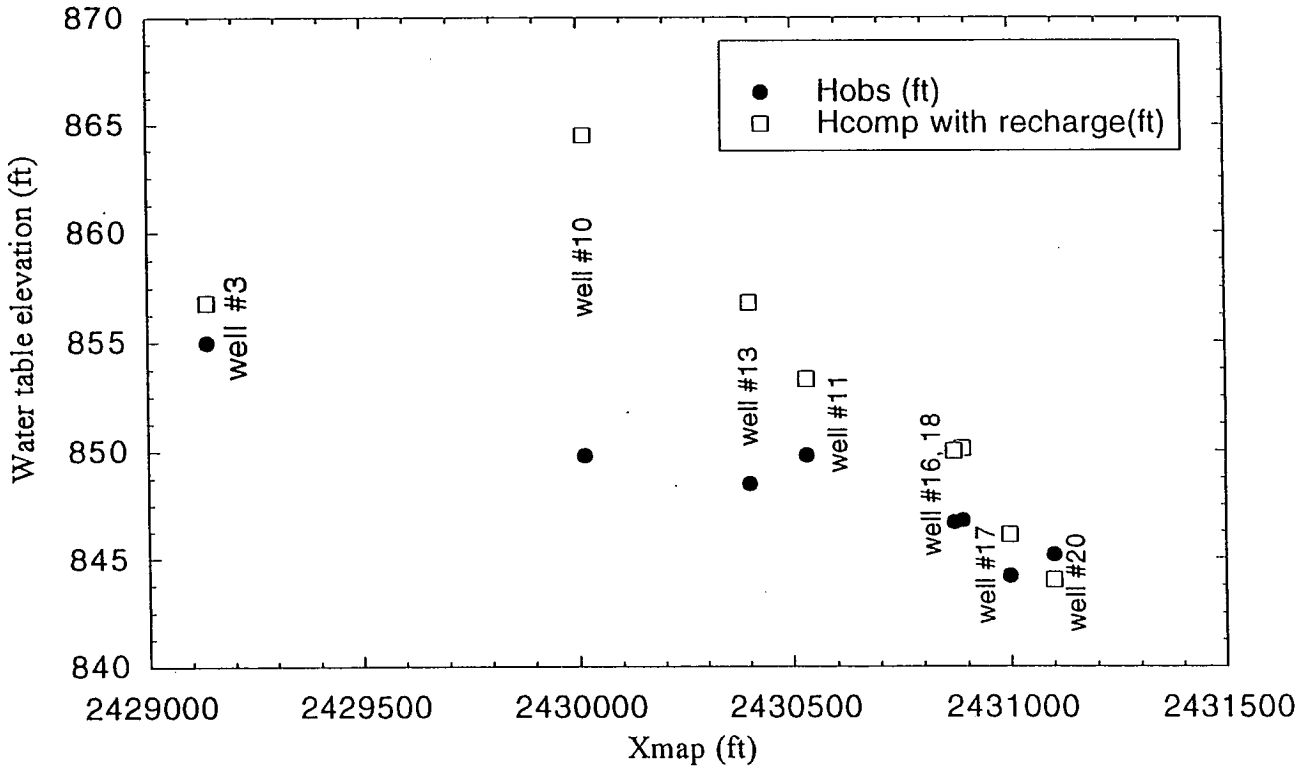

Fig. 1.15 Observed water table elevation compared to computed water elevation (Hcomp) with recharge= 2e-5 ft/s applied at cell 5

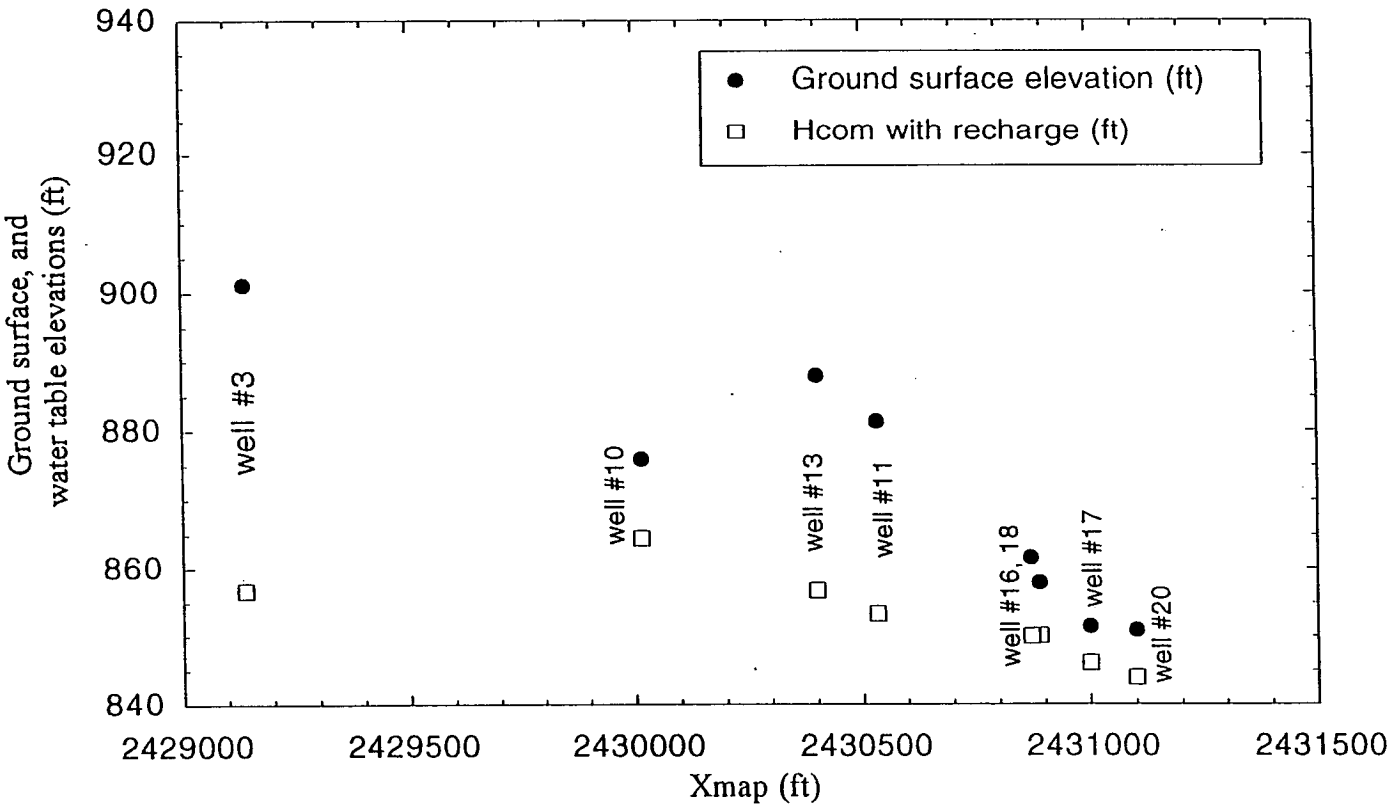

Fig. 1.16 Ground surface elevation compared to computed water elevation with recharge

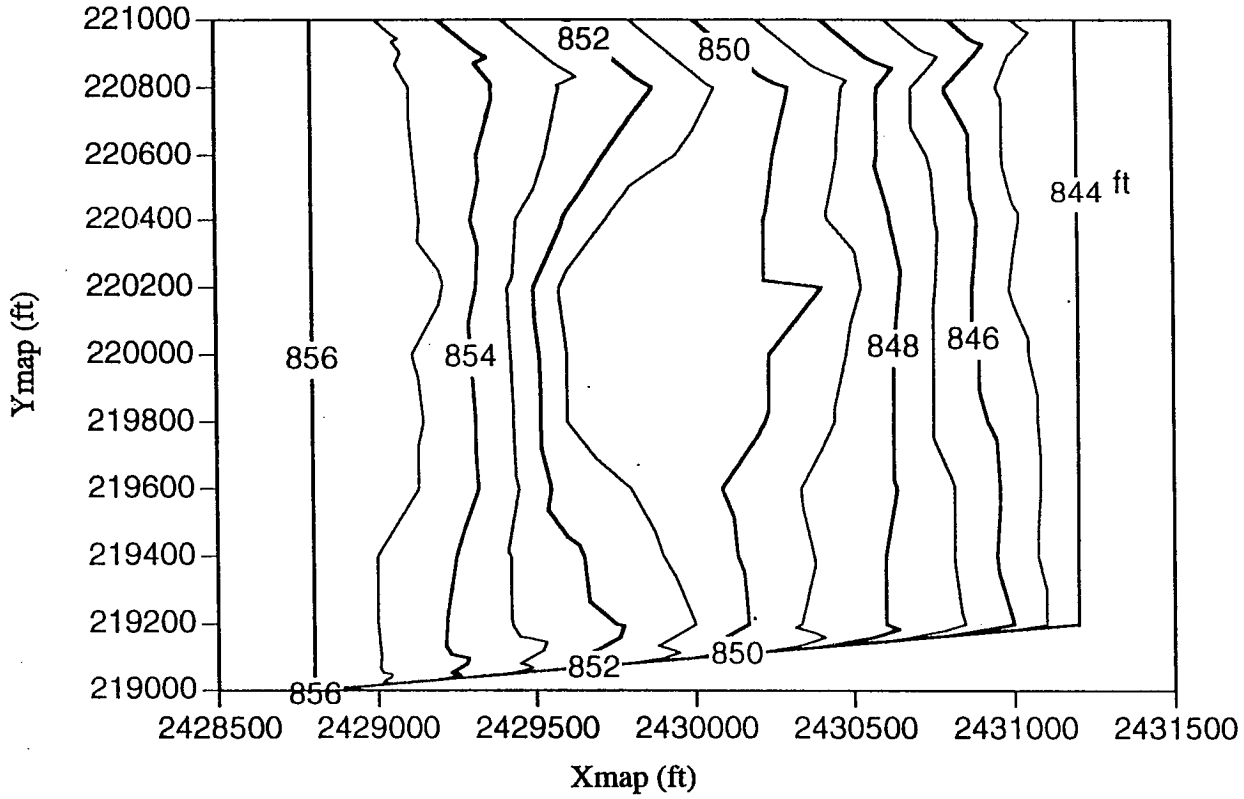

Fig. 1.17 Water table contours obtained from numerical flow simulation without recharge

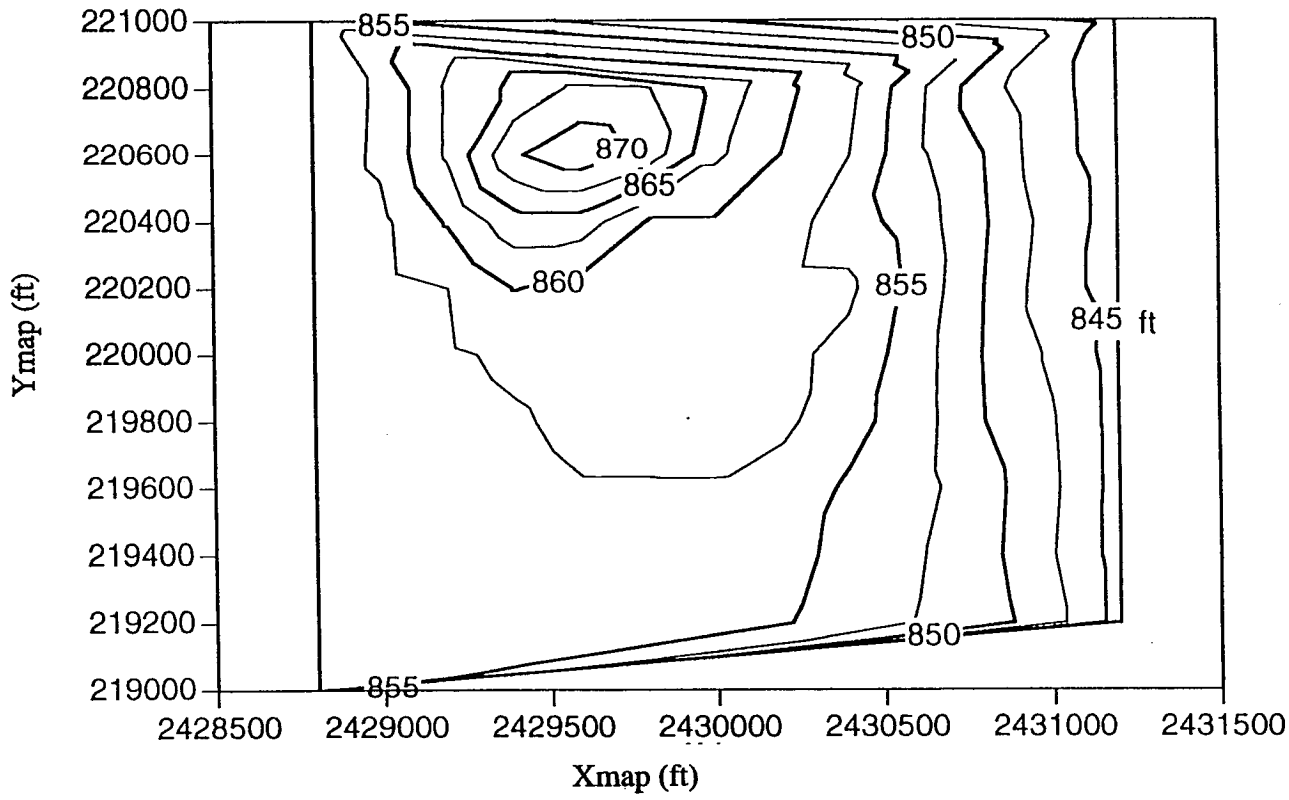

Fig. 1.18 Water table contours obtained from numerical simulation with recharge= 2e-5 ft/sec over cell 5

II. Numerical Simulation of Ground Water Mounding

2.1 Introduction

Ground water mounding is the rise of the water table above the regional level in an area of an aquifer in order to provide sufficient head to distribute the water supplied by a localized source (e.g., recharge from a spreading basin, waste water discharge system, irrigation, flooding, leakage from lagoon or land fill) to that area. The shape and height of the mound depend on many factors including source geometry, rate of recharge, geologic structure, hydraulic conductivity and its variations, flow/head controls and their location, saturated thickness, and regional flow in the aquifer. The flow pattern due to mounding transports and mixes substances, introduced by the recharge, with the ground water. Appropriate and properly applied models are useful in estimating the transport and fate of substances, designing remedial (cleanup) strategies, providing information for decision making, recognizing limitations of collected data, and guiding collection of new data. Prediction of ground water mounding is important in the design of water infiltration systems and of ground water remediation systems. However, it is difficult to accurately model such flow patterns and substance distributions numerically or analytically because detailed information on aquifer characteristics and properties is not usually available.

From a literature review, it was found that analytical solutions of ground water mounding are based upon linearization methods for simple cases (Haar, 1962; Dagan, 1967; Hantush, 1967; Huisman, 1972; and Brock, 1976; etc.). These analytical solutions are useful for initial estimation. On the other hand, numerical methods are employed to solve the non-linear, free surface boundary condition when the assumptions of linearization can not be used (Singh, 1976; MODFLOW, 1988;

and Tsay; et al, 1994; etc.). Though the non-linear free surface boundary condition can be solved by numerical methods, the geologic information is still unknown.

Deterministic models require fully defined aquifer information to carry out the computations. As aquifers are usually highly heterogeneous (Dagan, 1989; Sudicky, 1986; Scholle, et al., 1982), several approaches have been taken to provide complete information on an aquifer. The simplest way is to assume the heterogeneous aquifer is homogeneous, using a representative or effective hydraulic conductivity (e.g., based upon a pump test or simplified model of the heterogeneity (e.g., horizontally or vertically stratified aquifer)). This simplification can result in analytical free surface solutions under certain conditions (e.g., Dupuit assumption). This approach can be useful for a preliminary estimate. A more accurate estimate requires an estimate of the actual heterogeneity through the spatial distribution of hydraulic conductivity. Three approaches are widely used: stochastic method (Dagan, 1989); geostatistic method (Isaaks, et al., 1989); and geologic method. The stochastic method is useful in estimating the flow field for a large scale, flow domain, but it is not suitable to estimate a localized flow domain (i.e., where the scale of that domain is $\leq$ correlation length scale). Further, it does not apply for a single aquifer with a unique set of properties, as it represents the ensemble average of many realizations of an aquifer having a statistical distribution of properties. The geostatistic method is an interpolation process which estimates the unknown parameters of the flow domain from known points; a common method, kriging assumes that aquifer properties are from a second order, stationary distribution. Soil samples and properties from a boring usually provide the known information. Geologists also use soil samples from borings to obtain knowledge about erosion and deposition processes along with experience to configure the structure of an aquifer. For some sites an aquifer can be represented as isolated heterogeneities in a homogeneous aquifer or as discrete, contiguous, homogeneous facies (e.g., Underwood, et al., 1984). The particular pattern, geometry and hydraulic conductivity selected strongly affect the calculated ground water mounding and the flow pattern from local recharge. Hence, it is

essential to determine heterogeneity geometry and property effects on ground water mounding and the resulting flow pattern when deterministic methods are used.

The objectives of this research are to:

1) develop a numerical method for computing two- and three-dimensional ground water mounding using a transformation technique and finite differences, verify the two-dimensional model by Hele-Shaw results and determine the importance (or effect) of domain transformation in representing both heterogeneity and free surface; and

2) employ sensitivity analysis to determine the effects of position, geometry, orientation and hydraulic conductivity contrast of a single heterogeneity on ground water mounding and its flow pattern.

2.2 Methods

Transforming a problem involving a complex boundary shape (e.g., ducts, engine intakes, and complete aircraft or automobiles) and solving it in a regular domain is a technique that has been widely used. The procedure involves generating a grid in the physical domain, transforming the physical domain (Cartesian coordinate) into the computational domain (generalized curvilinear coordinate), and solving the problem in the computational domain. Grid generation for the physical domain is a key step to obtaining accurate, reasonable solutions.

2.2.1 Coordinate Transform

For the finite difference method, the imposition of boundary conditions on a domain of complex geometry requires a complicated interpolation of data on local grid lines (such as Singh, 1976) and typically, a local loss of accuracy in the

computational solution. Such difficulties motivated the introduction of a mapping or transformation from the physical domain (x, y, z -rectangular coordinate domain) to a computational domain (ξ, η, ζ -generalized coordinate domain). A distorted region in the physical domain is mapped into a rectangular region in generalized coordinate space (Fig. 2.1).

It is assumed that there is a unique, single-valued relation between the physical domain and the generalized coordinate domain; for a three-dimensional problem, these relations are

$$\xi = \xi(x,y,z),\ \eta = \eta(x,y,z) \text{ and } \zeta = \zeta(x,y,z) \tag{2.1}$$

with the inverse relations

$$x = x(\xi,\eta,\zeta),\ y = y(\xi,\eta,\zeta) \text{ and } z = z(\xi,\eta,\zeta) \tag{2.2}$$

The Jacobian matrix, $\underline{\underline{J}}$, and its inverse, $\underline{\underline{J}}^{-1}$ for these relations are

$$\underline{\underline{J}} = \begin{bmatrix} \frac{\partial \xi}{\partial x} & \frac{\partial \xi}{\partial y} & \frac{\partial \xi}{\partial z} \\ \frac{\partial \eta}{\partial x} & \frac{\partial \eta}{\partial y} & \frac{\partial \eta}{\partial z} \\ \frac{\partial \zeta}{\partial x} & \frac{\partial \zeta}{\partial y} & \frac{\partial \zeta}{\partial z} \end{bmatrix} \tag{2.3}$$

and

$$\underline{\underline{J}}^{-1} = \begin{bmatrix} \frac{\partial x}{\partial \xi} & \frac{\partial x}{\partial \eta} & \frac{\partial x}{\partial \zeta} \\ \frac{\partial y}{\partial \xi} & \frac{\partial y}{\partial \eta} & \frac{\partial y}{\partial \zeta} \\ \frac{\partial z}{\partial \xi} & \frac{\partial z}{\partial \eta} & \frac{\partial z}{\partial \zeta} \end{bmatrix}. \tag{2.4}$$

The elements of $\underline{\underline{J}}^{-1}$ can be related to the elements of $\underline{\underline{J}}$ by

$$\underline{\underline{J}} = \frac{\text{Transpose of Cofactor } (\underline{\underline{J}}^{-1})}{\left|\underline{\underline{J}}^{-1}\right|} \tag{2.5}$$

where

$$\left|\underline{\underline{J}}^{-1}\right| = x_\xi(y_\eta z_\zeta - y_\zeta z_\eta) - x_\eta(y_\xi z_\zeta - y_\zeta z_\xi) + x_\zeta(y_\xi z_\eta - y_\eta z_\xi). \tag{2.6}$$

2.2.2 Grid Generation

The computational grids in this work were generated by EagleView, developed by Mississippi State University. This software must be run on a Silicon Graphics Computer. It is a panel controlling code. The theoretical part of Eagle View is described by Thompson (1985). General rules for generating grids are based upon the following considerations: (1) limitation of computer memory, (2) point distribution, and (3) grid orthogonality.

2.2.3 Governing Equation

The governing equation of ground water mounding results from substituting Darcy's law into the equation of continuity; thus

$$\nabla \cdot \left(\underline{\underline{K}} \cdot \nabla \phi\right) = 0, \tag{2.7}$$

where $\underline{\underline{K}}$ is the hydraulic conductivity tensor, and ϕ is piezometric head. This equation can be expressed as

$$\frac{\partial}{\partial x}\left(K_{xx}\frac{\partial \phi}{\partial x}\right) + \frac{\partial}{\partial y}\left(K_{yy}\frac{\partial \phi}{\partial y}\right) + \frac{\partial}{\partial z}\left(K_{zz}\frac{\partial \phi}{\partial z}\right) = 0, \tag{2.8}$$

when the coordinate axes are aligned with the principal axes of $\underline{\underline{K}}$. For a homogeneous and isotropic porous medium, Eq. (2.8) becomes

$$\nabla^2\phi = 0 \tag{2.9}$$

which is Laplace's equation.

2.2.4 Free Surface Boundary Condition

The water table can also be determined by assuming that the aquifer is rigid and saturated below the water table, capillary effects are negligible, and water is incompressible and released instantaneously from storage with a decline in pressure. The free surface boundary conditions include: (i) zero pressure condition; and (ii) prescribed flux across this boundary.

(i) zero pressure condition

Applying the zero pressure condition on the free surface to the piezometric equation gives

$$\phi = z \tag{2.10}$$

which shows that the piezometric head on the free surface is equal to the elevation of the surface.

(ii) boundary of prescribed flux

a. without recharge

The unsteady free surface without recharge is a material surface which means that a fluid particle on the surface always stays on the surface. The free surface boundary

condition can be derived by applying the substantial derivative to the free surface function F to give

$$\frac{\partial F}{\partial t} + \underline{v} \cdot \nabla F = 0, \tag{2.11}$$

where $\underline{v}$ is the velocity of particles on the free surface.

b. with recharge

For the free surface with recharge, substitute

$$\underline{v} = \frac{\underline{q} - \underline{N}}{n_e} \tag{2.12}$$

into Eq. (2.11), where $\underline{N}$ is the vertical recharge rate, $\underline{N} = -N\underline{k}$. The free surface condition with recharge is

$$\frac{\partial F}{\partial t} + \left(\frac{\underline{q} - \underline{N}}{n_e} \right) \cdot \nabla F = 0 \tag{2.13}$$

2.2.5 Numerical Implementation

As the problem is solved in the generalized coordinate domain, the governing equation and free surface boundary condition are transformed to the ξ, η, ζ coordinates by applying the chain rule. For the two-dimensional problem, a 9-point scheme was used (Fig. 2.2). For the three-dimensional problem, a 19-point scheme was used (Fig. 2.3). As an iteration algorithm was used to predict the free surface location, the initial guess of the free surface is important to get the correct solution and to reduce the iterations for convergence.

2.2.6 Algorithms

a. steady state

A shooting method is used in which the necessary conditions of the free surface are obtained by iteration.

The algorithm for the steady-state is described as follows:

step 1: compute initial guess of the water table profile by Dupuit assumption ($H_{I,J}$)

step 2: construct grid for computation and calculate transformation relation based on the geometry of aquifer domain

step 3: solve the flow domain potential ($\phi_{I,J,K}$) according to the governing equation and boundary conditions

step 4: find the maximum difference between $H_{I,J}$ and $\phi_{I,NY}$ - $Max\left|\phi_{I,J,NZ} - H_{I,J}\right|$ and check convergence. If it is satisfied, go to step 5; if not, compute $H_{I,J}^{new} = \left(H_{I,J}^{old} + \phi_{I,J,NZ}\right)/2$ and go to step 2

step 5: output results

The convergence tolerance is set to be 10^{-6} to avoid machine error with double precision calculations.

b. unsteady state

An explicit method is used for calculating the water table location at time k'+1. Rearrange Eq. (2.13), and separate it into the form

$$\Delta\phi = \frac{\Delta t}{n_e} F, \tag{2.14}$$

where n_e is the effective porosity and F is the equation of the rising water table due to recharge in time Δt. Then,

$$H_{I,J}^{k'+1} = \phi_{I,J,NZ}^{k'+1} = \phi_{I,J,NZ}^{k'} + \frac{\Delta t \cdot F^{k'}}{n_e} \tag{2.15}$$

A rigid lid approach is applied to estimate the free surface location for each time step. The steps of calculation are

step 1: free surface boundary at time k'+1 is calculated by Eq. (2.14) using internal flow information at time k'

step 2: internal flow at time k'+1 is calculated by the governing equation using the free surface boundary as a constant head boundary from step 1

step 3: free surface boundary at time k'+1 is calculated using the internal flow solution from step 2

step 4: compare the free surface boundary values in steps 1 and 3. If $Max\left(\left|\phi_{I,J,NZ}^{new} - \phi_{I,J,NZ}^{old}\right|\right) \le \varepsilon$ then go to step 1

step 5: if step 4 is not satisfied, then calculate the internal flow at time k'+1 using the free surface boundary from step 3

step 6: calculate the free surface boundary at time k'+1 using the internal flow from step 5 and go to step 4 to check convergence

The convergence tolerance e is usually set equal to 10^{-6} to avoid machine error.

2.2.7 Flow Pattern

A particle tracking scheme is used to determine the flow pattern resulting from ground water mounding. Two things are important to be determined: the

distance upstream (of the mound) particles move and the maximum depth of penetration (of recharged water) below the water table. The particle tracking scheme uses the mounding velocity field as the input. A particle released at the upstream edge of the recharge area is tracked.

A fourth-order Runge-Kutta method (PATH3D) was used. The final position of a particle after each time step is calculated using an average involving four velocities. The final x-coordinate of a particle at the end of each tracking step is

$$x_p = x_0 + \frac{1}{6}(k + 2l + 2m + n) \tag{2.16}$$

where $k = \Delta t V(x_0), l = \Delta t V(x_1), m = \Delta t V(x_2), n = \Delta t V(x_3)$. $V(x_0)$ is the velocity in the x direction at the initial position (x_0) of the particle; $V(x_1)$ is the velocity at a position halfway between the initial position and the trial location $x_k = x_0 + k$; $V(x_2)$ is the velocity is the velocity at a position halfway between the initial position and the trial location $x_l = x_0 + l$; $V(x_3)$ is the velocity at $x_m = x_0 + m$.

The velocity field is known at the nodes only. Since the tracking position (x_p, y_p) is not necessarily located at a node, the velocity at (x_p, y_p) is estimated by Lagrange's interpolation method from its neighboring nodes.

2.3 Results and Discussion

2.3.1 Testing and Verification of Two-Dimensional Ground Water Mounding Model with Hele-Shaw Model

The two-dimensional ground water mounding model for a heterogeneous aquifer is compared with observations from a Hele-Shaw model. The purposes of this experiment are to test the numerical model, to determine an appropriate grid pattern for computation, and to verify this numerical model. Two aquifer formations were used in the experiments: (1) homogeneous aquifer; and (2) homogeneous aquifer with a single heterogeneity of rectangular shape.

The development of the equations describing flow in a Hele-Shaw model may be found in many places (e.g., Schlichting, 1960; Polubarinova-Kochina, 1962; Harr, 1962; Murray, 1970; and Bear, 1972). The equivalent hydraulic conductivity, K_m, for the Hele-Shaw (viscous flow analog) is

$$K_m = \frac{b^2 g}{12\nu}, \tag{2.17}$$

where b = spacing of plates and ν = kinematic viscosity of oil (fluid).

The Hele-Shaw model used is the one that Murray (1970) built and used for seepage face research. This model, consists of two parallel plates, upstream and downstream reservoirs and a motor-transmission-pump assembly. The two, closely-spaced, plastic (acrylic) plates are one-half inch thick, 30 inches high, and 8 feet long (Fig. 6.2). Murray found that a spacing of about 1/10 inch provided a negligible capillary rise (less than 1/10 inch). To facilitate construction, the spacing was designed to be 0.109 inch; 1/8" diameter rods were placed in a square grid (12" x 6.5") to help maintain a uniform spacing. On each end of the parallel plates is a reservoir made of ½ inch acrylic plastic sides, and on the bottom is a ½ inch aluminum plate. In order to simulate ground water mounding, recharge is added over a certain portion of the top of the Hele-Shaw model. A peristaltic pump supplies the constant (and adjustable) recharge rate from the reservoir below the Hele-Shaw model. The recharge flows vertically and freely to the free surface in the model. Hence, the flow rate is equivalent to the hydraulic conductivity (K_m). A flow rate less

than K_m is generated by developing a finite, perched aquifer above the water table. Since the head on the perched aquifer is not uniform, the recharge rate is not uniform. However, it was shown from this experiment that a uniform (average of the non-uniform pattern recharge from the simulated perched aquifer) yields a good estimate of the ground water mounding. Non-homogeneity in hydraulic conductivity is produced by changing the width between the plates. This variation was done by inserting into the space between the plates thin sheets of aluminum (held in place by applying plastic rubber on the corner of the aluminum) with thickness determined from $K_1/K_2 = (b_1/b_2)^2$, where 1 and 2 refer to the regions of reduced and regular hydraulic conductivity (Bear, 1972).

2.3.1.1 Homogeneous Aquifer

a. recharge rate equals hydraulic conductivity

Four mounding experiments using the Hele-Shaw model were done to verify the two-dimensional, numerical, ground water mounding model for a homogeneous aquifer. The first and second experiments were ground water mounding in a homogeneous aquifer without regional flow, $H_1 = H_2$ (H_1 and H_2 are the left and right boundary , constant heads, respectively). The third and fourth experiments were ground water mounding in a homogeneous aquifer with regional flow, $H_2 > H_1$. The third test had an average regional flow gradient of 9%, and the fourth test had a regional flow gradient of 7%. Comparisons between numerical results and Hele-Shaw model are shown in Figures 2.5 and 2.6 for experiments 1 and 3, respectively.

b. recharge rate less than hydraulic conductivity

Three experiments were done using a perched aquifer to generate a recharge rate less than the hydraulic conductivity (K_m). Fig. 2.7 is the comparison between numerical results and Hele-Shaw model for experiment 7.

2.3.1.2 Homogeneous Aquifer with Single Heterogeneity

A 30.5 cm long, 5.4 cm wide, 0.226 cm thick aluminum plate was inserted into the Hele-Shaw model with its center located 108.25 cm from the left boundary and 37.4 cm from the bottom. Oil was recharged for a length 4.3 cm (105 cm to 109.3 cm from the left boundary). The observed free surface and the numerical results are in good agreement (Fig. 2.8).

2.3.1.3 Discussion and Conclusions

The Hele-Shaw model is a very useful devise for generating and visualizing unconfined, ground water flows. From the analog relation, the simulated hydraulic conductivity is proportional to square of the spacing. The spacing of this model is the most difficult parameter to be controlled and measured.

Numerical and experimental results are in good agreement for the homogeneous aquifer and the aquifer with a single heterogeneity. The maximum height of mounding could not be observed when the recharge rate was equal to the simulated hydraulic conductivity as the area underneath the recharge area is saturated.

2.3.2 The Flow Pattern of Homogeneous and Isotropic Aquifer

Some particle tracking scheme results are shown in Figures 2.9 and 2.10, where H(x) is the free surface from the numerical results. Basic data for test 1 and 2 are given in Table 2.1. A particle was released at the left boundary of the recharge area. This particle stays at the free surface (flowing upstream) until the velocity of the x-component equals zero. This is the distance that particles move upgradient. The penetration depth is the maximum depth of recharged water when a particle moves parallel to the regional flow. Flow above the path line is caused by the recharge (mounding) and flow beneath the path line is caused by the regional flow. As the regional flow gradient of test 1 is larger than that of test 2, N/Q is smaller for test1

than for test 2. When the same recharge rate is applied to the aquifer, the particle in Fig. 2.10 flows to the left boundary (line for N/Q=3.035) but the particle in Fig. 2.9 is carried away with regional flow to the right boundary (line for N/Q=1.430).

2.3.3 Single Heterogeneity Effects on Ground Water Mounding

In order to quantify heterogeneity scale (size) effects on mounding, a dimensionless parameter was chosen as

$$\delta = \frac{1}{N_R}\sqrt{\sum_{I=1}^{N_R}\left(\frac{\phi_{I,NY} - H^D_{I,NY}}{H^D_{I,NY}}\right)^2}, \qquad (2.18)$$

where H^D is the free surface estimated by Dupuit assumption and N_R is the number of grid points of the recharge area. Because ground water mounding below the recharge area is more significant than at other locations, only mounding under the recharge area is considered. The synthetic aquifer is 100 m long and 40 m (= H_0) thick with hydraulic conductivity 1 cm/sec. The recharge rate is 0.5 cm/sec with a recharge length of 10 m. This recharge center is located at (50, 40). An elliptical heterogeneity was placed with its center located at (50, 30). The heterogeneity has long axis dimensions of 30m, 20m and 10m and short axis dimensions of 4m, 2m and 1m. Heterogeneity hydraulic conductivity ratios (heterogeneity / aquifer) 10^{-6}, 10^{-3}, 10^{-2}, 10^{-1}, 10^{0}, 10^{1}, 10^{2}, 10^{3}, and 10^{6} were used.

It can be seen from Fig. 2.11 that (1) δ is no longer affected by the hydraulic conductivity ratio if that ratio is greater than 10^2 or less than 10^{-3}; (2) vertical thickness of lense has some effect on ground water mounding; and (3) ground water mounding is affected more by hydraulic conductivity ratio < 1 (i.e., heterogeneity less conductive than aquifer) than by positive ratios.

2.4 Conclusions and Recommendations

2.4.1 Conclusions

1) Application of the generalized curvilinear coordinates to simulating ground water mounding is efficient for the numerical simulation convergence of the free surface, since grid points are located on the free surface.

2) Stability analysis was fulfilled by the CFL condition (Strikwerda, 1989). It was been found that it is not efficient to apply the maximum time step for calculation. Though the total time steps for the problem to reach a certain time are reduced when a larger time step is used, the number of iterations during each time step is greatly increased.

3) Numerical results were checked by the Hele-Shaw model. They are in good agreement for the homogeneous aquifer and the aquifer with a single heterogeneity. The maximum height of mounding could not be observed when the recharge rate was equal to the simulated hydraulic conductivity as the area under the recharge is saturated.

4) The fourth order Runge-Kutta particle tracking method gave reasonable results for the upgradient movement and penetration depth due to ground water mounding.

5) δ (Eq. (2.17)) is no longer affected by the hydraulic conductivity ratio if the ratio is $> 10^2$ or $< 10^{-3}$.

6) More complete results will be available in the Ph.D. thesis "Numerical simulation of ground water mounding" by T-S Tsay, expected in May 1995.

2.4.2 Recommendations

1) Effects of diffusion and dispersion should be considered in estimating solute distribution introduced by the recharge.

2) The dynamic grid of the free surface should be improved to be more orthogonal.

3) Block heterogeneity is assumed to have a single value of hydraulic conductivity so the hydraulic conductivity changes abruptly from one block to an adjacent block. Continuous changes in hydraulic conductivity from one block to another should be considered. Further, the hydraulic conductivity of a particular block could range within certain values so that the hydraulic conductivity of the whole flow domain is continuous.

4) Free surface movement through heterogeneities should be considered.

2.5 References

Bear, J. *Dynamics of fluids in porous media.* New York: Dover Publication, Inc.,764 pages. 1972.

Brock, R. R. "Dupuit-Forchheimer and potential theories for recharge from basins," *Water Resources Research* **12**(5, October), 1976, pp. 909-911.

Dagan, G. "Linearized solutions of free-surface groundwater flow with uniform recharge," *Journal of Geophysical Research* **72**(4, Feb.), 1967, pp. 1183-1193.

Dagan, G. *Flow and Transport in Porous Formations*. New York: Springer-Verlag, 461 pages. 1989.

Haar, M.E. *Ground Water and Seepage*. New York: McGraw-Hill Book Co. Inc. 1962.

Hantush, M. S. "Growth and Decay of Groundwater-mounds in Response to Uniform Percolation," *Water Resources Research* **3**(1), 1967, pp. 227-234.

Huisman, L. *Ground-Water Recovery*. Winchester Press, New York, 1972.

Isaaks, E. H. and Srivastava, R. M. *An Introduction to Applied Geostatistics*. New York: Oxford University Press, 561pages, 1989.

Murray,W.A. *Seepage Face Effects in Unsteady Groundwater Flow*. Ph.D. Thesis, Civil and Environmental Engineering, University of Wisconsin at Madison, 1970.

Polubarinava-Kochina, P.Ya. *Theory of Ground Water Movement.* Translated by J. DeWiest, Princeton: Princeton University Press, 1962.

Schlichting, H. *Boundary Layer Theory*. 7th Ed. Translated by J. Kestin, New York: McGraw-Hill, 1979.

Scholle, P. A. and Spearing, D. *Sandstone Depositional Environments*. Published by The American Association of Petroleum Geologists, Tulsa, Oklahoma. 1982.

Singh, R. "Prediction of Mound Geometry Under Recharge Basins," *Water Resources Research* **12**(4, August), 1976, pp. 775-780.

Sudicky, E. A. "A natural-gradient experiment on solute transport in a sand aquifer: spatial variability of hydraulic conductivity and its role in the dispersion process," *Water Resources Research*, 22, 1986, pp. 2069-2082.

Strikwerda, J. C. *Finite Difference Schemes and Partial Differential Equation.* Wadsworth & Brooks/Cole Advanced Books & Software, Thomson Information/Publishing Group, 1989, 386 pages.

Tsay, T-S; Hoopes, J. A.; Rashad, S.; and Majali, Y. "Modeling 3-D Ground water Mounding," *Proceedings of the Hydraulic Engineering*. Hydraulics Division of American Society of Civil Engineering, August, 1994.

Underwood, J. E. and Zenz, D. E. Rapid Infiltration System, Geotechnical Report, City of Lake Geneva, Wisconsin. Donohue, August, 1984.

Tables and Figures

	H_1 (cm)	H_2 (cm)	d (cm)	Lr (cm)	2w (cm)	gradient
test 1	41.4	52.3	243.5	106	6	4.5%
test 2	41.4	46.9	243.5	106	6	2.25%

Table 2.1 Particle tracking basic data of test 1 and 2

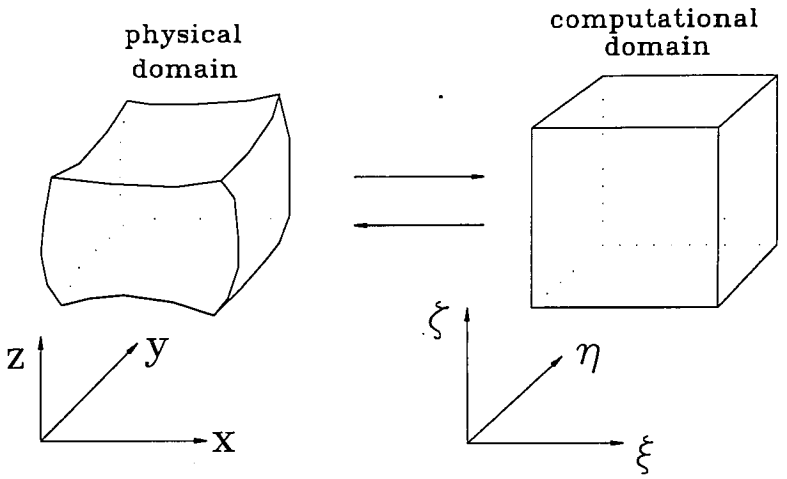

Fig. 2.1 Correspondence of the physical and generalized coordinate domain

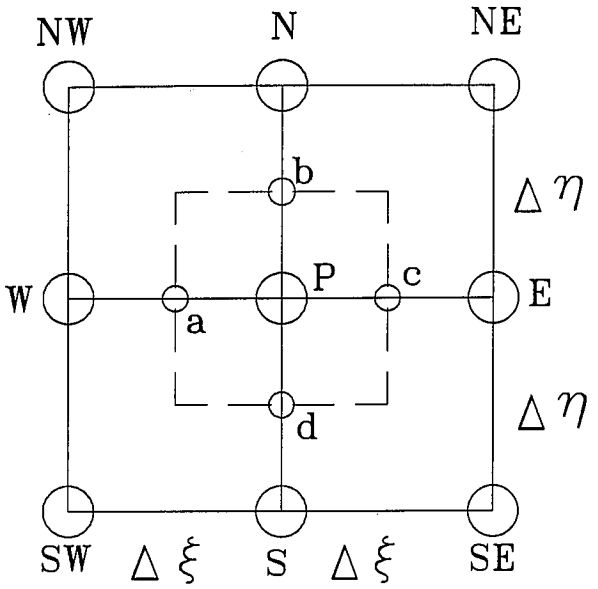

Fig. 2.2 Second order accurate nine-point scheme

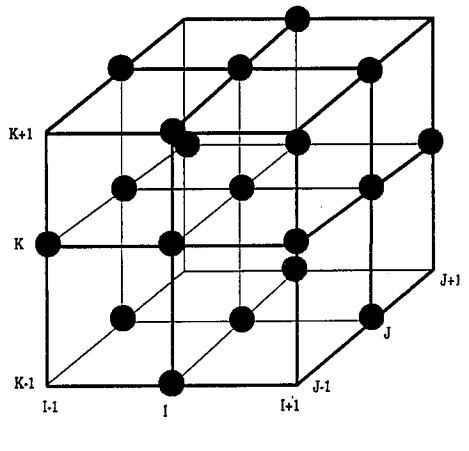

Fig. 2.3 Second order accurate 19-point scheme

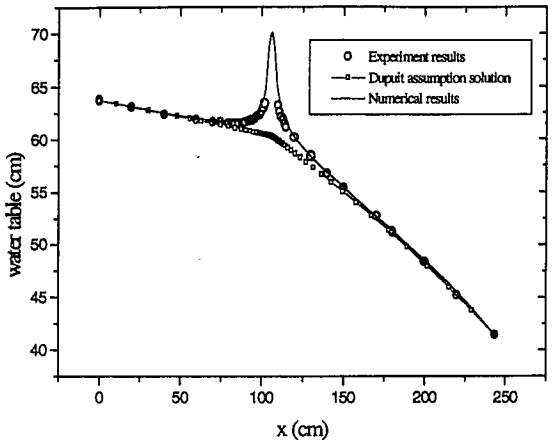

Fig. 2.6 Comparison of experimental results and numerical results of Experiment 3

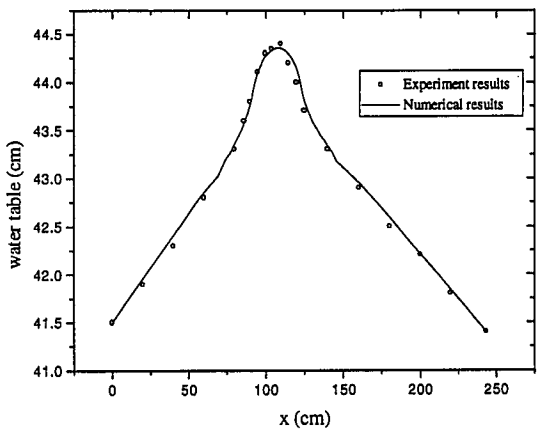

Fig. 2.7 Comparison of experimental results and numerical results of Experiment 7

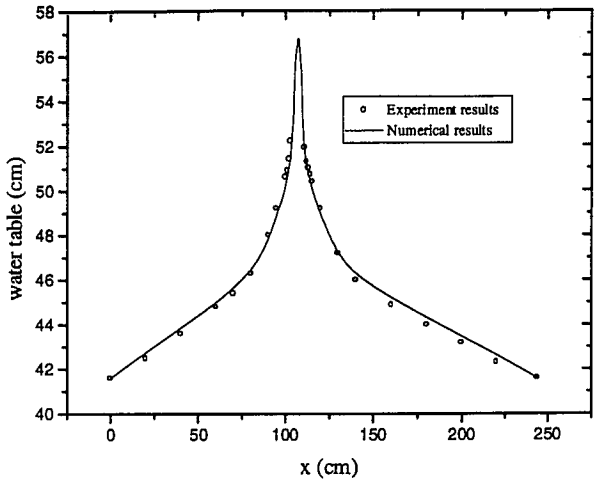

Fig. 2.8 Comparison of experimental results and numerical results of Experiment 8

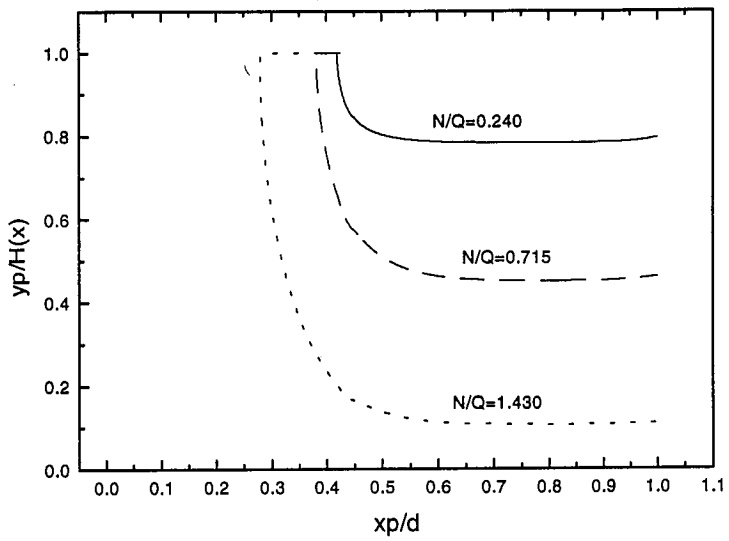

Fig. 2.9 Particle tracking for test 1

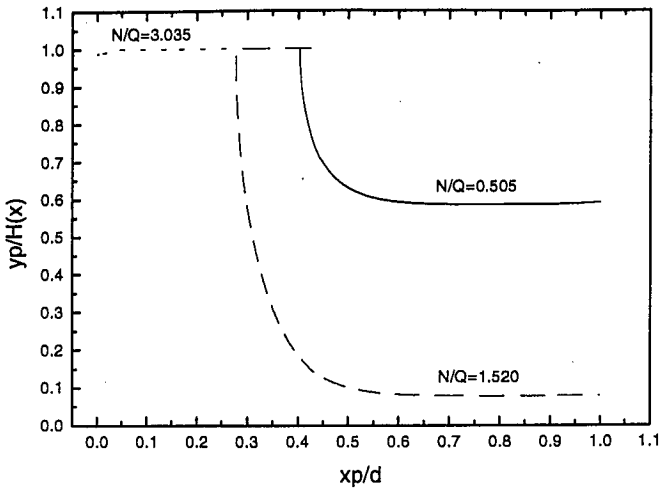

Fig. 2.10 Particle tracking for test 2

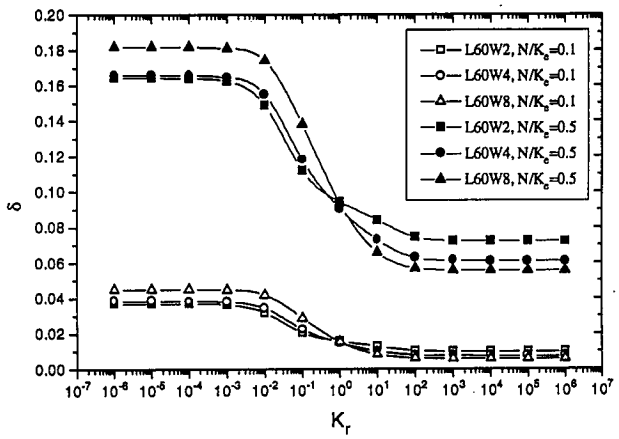

Fig 2.11 Deviation of numerical ground water mounding results from Dupuit solutionfor various heterogeneity scales (L60W8 means long axis is 60m and short axis is 8m)